

New insights into the atmospheric mercury cycling in Central Antarctica and implications at a continental scale

Hélène Angot¹, Olivier Magand^{2, 1}, Detlev Helmig³, Philippe Ricaud⁴, Boris Quennehen^{2, 1}, Hubert Gallée^{2, 1}, Massimo Del Guasta⁵, Francesca Sprovieri⁶, Nicola Pirrone⁷, Joël Savarino^{2, 1}, Aurélien Dommergue^{1, 2}

¹Univ. Grenoble Alpes, Laboratoire de Glaciologie et Géophysique de l'Environnement (LGGE), 38041 Grenoble, France.

²CNRS, Laboratoire de Glaciologie et Géophysique de l'Environnement (LGGE), 38041 Grenoble, France.

³Institute of Arctic and Alpine Research (INSTAAR), University of Colorado, Boulder, CO 80309-0450, USA.

⁴CNRM/GAME, Météo-France/CNRS, 42 avenue de Coriolis, 31057 Toulouse, France.

⁵CNR-Istituto Nazionale di Ottica, Largo E. Fermi 6, Firenze, 50125, Italy.

⁶CNR-Institute of Atmospheric Pollution Research, Division of Rende, Italy.

⁷CNR-Institute of Atmospheric Pollution Research, Montelibretti, Rome, Italy.

Correspondence to: A. Dommergue (aurelien.dommergue@ujf-grenoble.fr)

Abstract

Under the framework of the GMOS project (Global Mercury Observation System) atmospheric mercury monitoring has been implemented at Concordia Station on the high-altitude Antarctic plateau (75°06'S, 123°20'E, 3220 m above sea level). We report here the first year-round measurements of gaseous elemental mercury (Hg(0)) in the atmosphere and in snowpack interstitial air on the East Antarctic ice sheet. This unique dataset shows evidence of an intense oxidation of atmospheric Hg(0) in summer (24-hour daylight) due to the high oxidative capacity of the Antarctic plateau atmosphere at this period of the year. Summertime Hg(0) concentrations exhibited a pronounced daily cycle in ambient air with maximal concentrations around midday. Photochemical reactions and chemical exchange at the air/snow interface were prominent, highlighting the role of the snowpack on the

30 atmospheric mercury cycle. Our observations reveal a 20 to 30% decrease of atmospheric
31 Hg(0) concentrations from May to mid-August (winter, 24-h darkness). This phenomenon has
32 not been reported elsewhere and possibly results from the dry deposition of Hg(0) onto the
33 snowpack. We also reveal the occurrence of multi-day to weeklong atmospheric Hg(0)
34 depletion events in summer, not associated with depletions of ozone, and likely due to a
35 stagnation of air masses above the plateau triggering an accumulation of oxidants within the
36 shallow boundary layer. Our observations suggest that the inland atmospheric reservoir is
37 depleted in Hg(0) in summer. Due to katabatic winds flowing out from the Antarctic plateau
38 down the steep vertical drops along the coast and according to observations at coastal
39 Antarctic stations, the striking reactivity observed on the plateau most likely influences the
40 cycle of atmospheric mercury at a continental scale.

41

42 **1 Introduction**

43 Mercury biomagnifies in its methylated form in aquatic food webs to elevated levels in
44 freshwater and marine fish, causing adverse health effects to wildlife and humans (Mason et
45 al., 2012). In 2013, the Minamata Convention (UNEP, 2013) was adopted and opened for
46 signature to reduce the exposure of populations to this worldwide contaminant. Gaseous
47 elemental mercury (Hg(0)), the most abundant form of mercury in the atmosphere, is
48 efficiently transported around the globe, and even remote areas receive significant inputs of
49 anthropogenic mercury by long-range atmospheric transport, as recently reported in modeling
50 and observational studies (Weiss-Penzias et al., 2007; Lin et al., 2010).

51 Hg(0) can be oxidized into highly reactive and water-soluble gaseous and/or particulate
52 divalent species (Hg(II) and Hg(p), respectively) (Lin and Pehkonen, 1999) leading to the
53 formation and subsequent deposition of reactive mercury onto environmental surfaces
54 (Hedgecock and Pirrone, 2004). Upon deposition mercury can be reemitted back to the
55 atmosphere or may enter the food chain through the conversion of Hg(II) to its methylated
56 form (Driscoll et al., 2013). Effects and toxicity of mercury depends on this complex cycle,
57 which is still not fully understood, and are only indirectly related to regional and global
58 emissions (Driscoll et al., 2013). A better understanding of atmospheric mercury chemistry
59 will lead to improved global transport and deposition models and could help refine pollution-
60 control strategies around the world.

61 New oxidation pathways, discovered in 1995 in the Arctic (Schroeder et al., 1998) and
62 highlighting the influence of halogen radicals on Hg(0) oxidation in spring, changed our
63 understanding of the mercury cycle. While the Arctic has been extensively monitored, there is
64 still much to be learned from the Antarctic continent where studies are scarce (Dommergue et
65 al., 2010), especially on the high altitude plateau (see Fig. 1). The Antarctic plateau – ice-
66 covered area of ~ 7 million km² – was first considered to be chemically-inactive and a giant
67 cold trap for atmospheric species (e.g., Lambert et al., 1990). It turned out to be highly
68 photochemically active (Davis et al., 2001; Grannas et al., 2007) during the sunlit period with
69 oxidant concentrations approaching those of tropical or urban mid-latitude environments
70 (Eisele et al., 2008; Kukui et al., 2014). Earlier studies (Brooks et al., 2008; Dommergue et
71 al., 2012) – the only two mercury studies ever carried out on the high-altitude Antarctic
72 plateau with modern instruments – also suggested, based on short-term observations (a few
73 weeks) in summer, an intense reactivity of mercury on the plateau at the air/snow interface. In
74 this context, and under the framework of the GMOS project (Global Mercury Observation
75 System, www.gmos.eu), atmospheric mercury was continuously monitored at Concordia
76 Station (see Fig. 1) since 2012 and, for the first time, Hg(0) has been monitored year-round in
77 both the snow interstitial air and the overlying atmosphere in 2013. Given harsh weather
78 conditions (see section 2.1), and technical and logistical limitations, presenting such a record
79 is in itself an important achievement. The main objective of this study is to provide new
80 insights into the year-round cycling of gaseous mercury on the Antarctic plateau.

81

82 **2 Experimental Section**

83 **2.1 Sampling site**

84 Year-round measurements of gaseous mercury were conducted in 2012 and 2013 at the
85 French/Italian Concordia Station (75°06'S, 123°20'E, 3220 m above sea level), located on the
86 Antarctic plateau, 1100 km away from the nearest coast of East Antarctica (see Fig. 1).
87 Concordia Station is a regional topographic maximum on the plateau; the surface terrain
88 slopes do not exceed 1% (Genthon et al., 2010). The air temperature ranges between -20 °C in
89 summer and -70 °C in winter, with an annual mean value of -45 °C (Pietroni et al., 2012).
90 There is permanent daylight in summer and permanent darkness in winter. Snow
91 accumulation is ~ 10 cm/year (Genthon et al., 2013).

92 **2.2 Sampling instrumentation**

93 Instrumentation was located in a below-surface shelter at the edge of the “clean area”, 800 m
94 away from the main camp and upwind with respect to the dominant wind direction (south
95 west). In 2012, year-round measurements were performed in the atmospheric boundary layer
96 at about 500 cm above the snow surface. In 2013, measurements were performed in both the
97 atmosphere and in snowpack interstitial air for several trace gases including gaseous mercury
98 and ozone (O₃). Sampling instrumentation included one 10 m meteorological tower for above-
99 surface gradient sampling and two multi-inlet snow sampling manifolds (“snow towers”) for
100 measuring trace gases at various depths in interstitial air (Bocquet et al., 2007; Seok et al.,
101 2009). The 10 m meteorological tower was installed ~ 15 m upwind of the underground
102 instrument shelter. It accommodated three gas inlets at 1070 cm, 210 cm, and 25 cm above the
103 snow surface (see Fig. 2a). Trace gas measurements were acquired on each snow tower at six
104 height levels: 50 and 10 cm above the snow surface, and 10, 30, 50, and 70 cm below the
105 snow surface (see Fig. 2b). Sampling lines were purged continuously at 5 L/min on the
106 meteorological tower and intermittently at ~ 2-3 L/min on the snow towers. On each snow
107 tower, inlets were fitted with a small glass fiber filter in PTFE housing (25 mm Acrodisc
108 syringe filters, Pall Life Sciences, Ann Arbor, Michigan, USA) to prevent snow crystals from
109 entering the PFA sampling lines. Sampling lines were inside insulation tubing and the
110 temperature of the sampling lines was maintained at a level 5-10 °C warmer than the
111 snowpack temperature with a heat trace to prevent water vapor from freezing and clogging the
112 lines. An automatic sampling pattern was implemented: trace gases were collected
113 sequentially from the uppermost inlets on the meteorological tower to deepest levels of the
114 snow towers. Measurements were taken for 10 min from each inlet.

115 **2.3 Gaseous mercury measurements**

116 Measurements were performed using a Tekran 2537A analyzer (Tekran Inc., Toronto,
117 Canada) based on the amalgamation of mercury onto a gold cartridge followed by thermal
118 desorption and detection by an integrated cold vapor atomic fluorescence spectrometer
119 (CVAFS) at 253.7 nm (Fitzgerald and Gill, 1979; Bloom and Fitzgerald, 1988). The presence
120 of two gold cartridges allowed alternating sampling and desorption modes and thus a
121 continuous analysis in the pre-filtered (0.45 µm PTFE filter) and unheated sample air stream.
122 The sampling resolution was 5 min with a sampling flow rate of 0.8 L/min. Concentrations
123 are expressed in nanograms per cubic meter at standard temperature and pressure (273.15 K,

124 1013.25 hPa). Using both a 0.45 μm PTFE filter at the entrance inlet of the sample line, and
125 an unheated $\frac{1}{4}$ "PTFE sample line, we assume that only Hg(0) (vs. total gaseous mercury,
126 defined as the sum of gaseous mercury species) was efficiently collected and subsequently
127 analyzed in this study (Steffen et al., 2002; Temme et al., 2003; Steffen et al., 2008).

128 *Quality assurance and quality control procedures*

129 An automatic calibration step of the Tekran 2537A analyzer was carried out every 25 h with
130 an internal mercury permeation source. External calibrations were performed twice a year by
131 manually injecting saturated mercury vapor taken from a temperature-controlled vessel
132 (Tekran 2505 mercury vapor calibration unit, Hamilton digital syringe). As described by
133 Angot et al. (2014), bi-monthly to monthly routine maintenance operations were performed. A
134 software program was developed at the LGGE (Laboratoire de Glaciologie et Géophysique de
135 l'Environnement) in accordance with quality control practice in well-established North
136 American networks (Steffen et al., 2012). Based on various flagging criteria (Munthe et al.,
137 2011; D'Amore et al., 2015), it enabled rapid data processing in order to produce clean time
138 series of Hg(0). The detection limit is estimated at 0.10 ng/m^3 (Tekran, 2011). Based on
139 experimental evidence, the average systematic uncertainty for Hg(0) measurements is of ~ 10
140 % (Slemr et al., 2015).

141 **2.4 Surface snow sampling and analysis**

142 Surface snow samples (first cm) were collected weekly from February 2013 to January 2014
143 using acid cleaned PTFE bottles and clean sampling procedures. Upon collection, samples
144 were stored in the dark at $-20\text{ }^\circ\text{C}$. Field blanks, carried out by opening and closing a bottle
145 containing mercury-free water, were regularly conducted. Surface snow samples and field
146 blanks were analyzed for total mercury using a Tekran Model 2600. The instrument was
147 calibrated with the NIST SRM-3133 mercury standard. Quality assurance and quality control
148 included the analysis of analytical blanks, replicates, and internal standards (Reference Waters
149 for mercury: HG102-2 at 22 ng/L from Environment Canada). The limit of quantification –
150 calculated as 10 times the standard deviation of a set of 3 analytical blanks – amounted to 0.3
151 ng/L with a relative accuracy of $\pm 8\%$.

152 **2.5 Ancillary parameters**

153 *Ozone*

154 Measurements were performed using a UV absorption monitor (Thermo Electron
155 Corporation, Franklin, MA), model 49I in 2012 (Legrand et al., 2016) and model 49C in
156 2013. In 2013, the instrument was calibrated against the National Oceanic and Atmospheric
157 Administration Global Monitoring Division, Boulder, Colorado, standard.

158 *Air mass back trajectories*

159 Air mass back trajectories were computed using the Lagrangian model FLEXPART (Stohl et
160 al., 1998; Stohl and Thomson, 1999; Stohl et al., 2005) run in the backward mode and driven
161 by NCEP (National Center for Environmental Predictions) GFS (Global Forecast System)
162 final meteorological fields. Simulations were done every day at 1200 UTC in 2012 and 2013.
163 For each simulation, 20000 pseudo-particles were released by the model around the position
164 of Concordia Station and tracked for 5 days in three layers of altitude (0-0.1, 0.1-4 and 4-10
165 km above ground level). Simulations at an altitude of 4-10 km were computed in order to
166 investigate the potential occurrence of upper troposphere/lower stratosphere intrusions. For
167 each 1-h time step, the model produced a normalized particle residence time (in seconds)
168 within an output grid of $0.5 \times 0.5^\circ$. The sum of the 5 days outputs provided potential emission
169 sensitivities (PES, in seconds) for the three layers of altitude. PES in a particular grid cell is
170 proportional to the particle residence time in that cell. It should be noted that, in Antarctica,
171 the meteorological data driving the FLEXPART transport model rely on sparse
172 measurements. Consequently, the trajectories calculated in this region are often associated
173 with relatively high uncertainties.

174 *Height of the boundary layer and shortwave radiation*

175 The height of the boundary layer and downwelling shortwave radiation were calculated by the
176 MAR regional atmospheric model (Modèle Atmosphérique Régional). MAR was developed
177 at the LGGE for Polar Regions and the simulations have been evaluated against
178 meteorological observations made at Concordia Station (Gallée and Gorodetskaya, 2010;
179 Gallée et al., 2015).

180 *Meteorological data*

181 Temperature, wind speed and direction were recorded at six height levels on a 45 m tower.
182 The general observation set up is described by Genthon et al. (2010).

183 *Ice precipitation*

184 A tropospheric depolarization LIDAR (Light Detection And Ranging) operating at 523 nm
185 provided tropospheric profiles of aerosol and clouds every 5 min allowing detection of
186 water/ice clouds, snow drift, diamond dust and pollution plumes.

187 *Tropospheric temperature and integrated water vapor*

188 A H₂O Antarctica Microwave Stratospheric and Tropospheric Radiometers (HAMSTRAD)
189 instrument was used for the detection of the 60-GHz oxygen and the 183-GHz water vapor
190 lines allowing measurement of tropospheric temperature and water vapor profiles,
191 respectively, together with integrated water vapor (IWV) every 7 min. The instrument is fully
192 automated and a liquid nitrogen calibration is performed twice per year (Ricaud et al., 2015)

193 *Eddy diffusivity and friction velocity*

194 The Eddy diffusivity was calculated as follows (Xiao et al., 2014):

$$195 \quad K = k u_* z / \varphi_h \quad (1)$$

196 where k (set to 0.40) is the von Karman constant, u_* the friction velocity (m/s), z the
197 measurement height (m), and φ_h the Obukhov stability function. According to Frey et al.
198 (2013), the stability function was $\varphi_h = 0.95 + 4.62 \frac{z}{L}$ for stable conditions above snow (King
199 and Anderson, 1994), and $\varphi_h = 0.95 \left(1 - 11.6 \frac{z}{L}\right)^{-0.5}$ for unstable conditions (Hoegstroem,
200 1988). u_* and L (the Obukhov length (m)) were computed from the three-dimensional wind
201 components (u , v , w) and temperature measured by a Metek sonic anemometer mounted at 8
202 m above the snow surface.

203

204 **3 Results and Discussion**

205 **3.1 Hg(0) concentrations in ambient air**

206 The record of atmospheric Hg(0) over the entire 2012-2013 period is displayed in Fig. 3a.
207 Hg(0) concentrations ranged from below 0.10 to 2.30 ng/m³, with average values amounting
208 to 0.76 ± 0.24 ng/m³ in 2012, and to 0.81 ± 0.28 ng/m³, 0.84 ± 0.27 ng/m³, and 0.82 ± 0.26
209 ng/m³ in 2013 at 25, 210, and 1070 cm above the snow surface, respectively. No significant
210 difference was observed between annual averages of Hg(0) concentrations measured at the
211 three inlets of the meteorological tower in 2013 (p value = $3.1 \cdot 10^{-14}$, Mann-Whitney test). It
212 should be noted that Hg(0) concentrations at the three inlets were significantly different in

213 winter only (see section 3.1.4). These mean annual Hg(0) concentrations are lower than
214 annual averages reported at near-coastal or coastal Antarctic stations (i.e., $0.93 \pm 0.19 \text{ ng/m}^3$
215 for Hg(0) at Troll (Pfaffhuber et al., 2012) and $1.06 \pm 0.24 \text{ ng/m}^3$ for total gaseous mercury at
216 Neumayer (Ebinghaus et al., 2002)).

217 The seasonal boundaries are defined according to the transitions in downwelling shortwave
218 radiation (see Fig. 3b) as follows: winter from May to mid-August, spring from mid-August
219 to October, summer from November to mid-February, and fall from mid-February to April.
220 Unlike in winter, Hg(0) concentrations were highly variable during the sunlit period with
221 concentrations ranging from below 0.10 ng/m^3 to $1.50\text{-}2.00 \text{ ng/m}^3$, up to twice the average
222 background levels recorded in the Southern Hemisphere mid-latitudes (Slemr et al., 2015).
223 These seasonal features, in good agreement with observations at other Antarctic stations
224 (Ebinghaus et al., 2002; Pfaffhuber et al., 2012), suggest the existence of a photochemically-
225 induced reactivity of atmospheric mercury during the sunlit period. The mechanisms which
226 cause the seasonal variation of Hg(0) concentrations are discussed in the following sections.

227 **3.1.1 Spring**

228 First discovered in the Arctic (Schroeder et al., 1998), atmospheric Hg(0) depletion events
229 (AMDEs) result from an oxidation by reactive bromine species released during springtime so-
230 called “bromine explosions” in coastal regions (Durnford and Dastoor, 2011 and references
231 therein) and are concurrent with tropospheric O₃ depletion events (Simpson et al., 2007).
232 Despite the distance of Concordia Station from the coast (1100 km), a Hg(0) depletion event
233 was observed on 11 September 2013 due to a maritime air transport event (see Fig. 4a).
234 During this event, Hg(0) concentrations dropped from 0.85 to 0.56 ng/m^3 and exhibited a
235 strong positive correlation with O₃ mixing ratios ($\rho = 0.94$, p value = 5.10^{-7}).

236 **3.1.2 Summertime**

237 a) Oxidation of Hg(0) in ambient air and Hg(II) deposition onto snowpack

238 In summer, the mean atmospheric Hg(0) concentration was $0.69 \pm 0.35 \text{ ng/m}^3$ (mean \pm
239 standard deviation). This means that Hg(0) concentrations are $\sim 25\%$ lower than levels
240 recorded at the same period of the year at coastal Antarctic stations (Ebinghaus et al., 2002;
241 Sprovieri et al., 2002; Pfaffhuber et al., 2012). Total mercury concentrations in surface snow
242 samples were highly variable (median value: 4.8 ng/L , range: $< \text{detection limit} - 73.8 \text{ ng/L}$,
243 see Fig. 5) and were higher in summer (median value: 10.4 ng/L , range: $1.3 - 73.8 \text{ ng/L}$),

244 suggesting that divalent mercury species were preferentially deposited onto the snowpack at
245 this period of the year. The lower Hg(0) concentrations in ambient air along with high total
246 mercury concentrations in surface snow samples suggest an intense oxidation of Hg(0) in
247 ambient air in summer, followed by the deposition of oxidation products on surface snow.
248 This hypothesis is further supported by elevated oxidized mercury concentrations measured
249 on the Antarctic plateau at South Pole in summer ($0.10 - 1.00 \text{ ng/m}^3$) by Brooks et al. (2008).
250 The oxidative capacity of the Antarctic plateau atmosphere is elevated in summer, as
251 evidenced by several studies (Davis et al., 2001; Grannas et al., 2007; Eisele et al., 2008;
252 Kukui et al., 2014), likely explaining this intense oxidation of Hg(0) in ambient air. Among
253 these oxidants, NO_2 , RO_2 , and OH are particularly abundant at Concordia Station in summer
254 (Frey et al., 2013; Kukui et al., 2014) and a recent study provided as a first estimate a BrO
255 mixing ratio of 2-3 pptv near the ground during sunlight hours (Frey et al., 2015). Given the
256 current understanding of mercury oxidation and the lack of continuous halogens
257 measurements, we were not able to identify the exact mechanism for the reactivity observed at
258 Concordia Station. A two-step oxidation mechanism, favored at cold temperatures, is worth
259 being considered further. The initial recombination of Hg(0) and Br is followed by the
260 addition of a second radical (e.g., I, Cl, BrO, ClO, OH, NO_2 , or HO_2) in competition with
261 thermal dissociation of the HgBr intermediate (Goodsite et al., 2004; Wang et al., 2014).
262 According to Dibble et al. (2012), HO_2 , NO, NO_2 , and NO_3 bind Hg(0) too weakly to initiate
263 its oxidation in the gas phase and reactions of the HgBr intermediate with NO_2 , HO_2 , ClO,
264 and BrO are more important than with Br and OH. Further modeling or laboratory chamber
265 studies investigating the fate of Hg(0) in the presence of various potential oxidants are needed
266 to improve our understanding of the mechanisms.

267 b) Multi-day depletion events of atmospheric Hg(0)

268 From 19 January to 8 February 2012 and from 5 to 20 February 2013 we observed Hg(0)
269 depletion events. The mechanism seems however different from springtime AMDEs (see
270 section 3.1.1). While atmospheric Hg(0) concentrations dropped and remained low ($0.39 \pm$
271 0.19 ng/m^3 from 19 January to 8 February 2012, $0.41 \pm 0.21 \text{ ng/m}^3$ from 5 to 20 February
272 2013) for several weeks (see Figs. 3a, 6a, and 6e), O_3 showed no abnormal variability (see
273 Figs. 6d and 6h). These depletion events occurred as air masses stagnated over the Antarctic
274 plateau (see Figs. 4b and 4c) according to our FLEXPART simulations. This stagnation of air
275 masses is confirmed in 2013 (see Figs. 6f and 6g) by a decrease of temperature at 10 m a.g.l
276 (from $-29 \pm 3 \text{ }^\circ\text{C}$ in January to $-43 \pm 4 \text{ }^\circ\text{C}$ during the Hg(0) depletion event) and a low

277 integrated water vapor ($0.40 \pm 0.13 \text{ kg/m}^2$ during the Hg(0) depletion event vs. 0.77 ± 0.20
278 kg/m^2 in January). In both 2012 and 2013, depletions of Hg(0) ended when air masses started
279 moving out of the plateau (see Figs. 4d and 4e).

280 While previous studies attributed high Hg(II) concentrations in the Antarctic summer to
281 subsiding upper tropospheric air (Holmes et al., 2006; Brooks et al., 2008), potential emission
282 sensitivities suggest that the depletions of Hg(0) reported here were unlikely concomitant with
283 upper troposphere/lower stratosphere intrusions (see Figs. 4b and 4c, PES at 4-10 km). This is
284 also confirmed by stable O₃ mixing ratios. High altitude vertical profiles of Hg(0) should be
285 carried out to rule out this hypothesis of subsiding upper tropospheric air. We suggest that
286 these Hg(0) depletion events observed at Concordia Station result from processes occurring
287 within the shallow boundary layer. Since O₃ was not depleted during these events, Hg(0)
288 depletion cannot be accounted for by bromine oxidation alone. FLEXPART simulations along
289 with integrated water vapor and temperature measurements indicate that these Hg(0) depletion
290 events occurred as air masses stagnated over the Antarctic plateau. As highlighted in the
291 previous section, the oxidative capacity is high in summer on the plateau (Davis et al., 2001;
292 Grannas et al., 2007; Eisele et al., 2008; Kukui et al., 2014). This air mass stagnation might
293 favor an accumulation of oxidants within the shallow boundary layer (< 300 m in average),
294 leading to an oxidation of Hg(0) stronger than usual.

295 c) Hg(0) diurnal cycle

296 Based on a week of measurements made at Concordia Station in January 2009, Dommergue et
297 al. (2012) reported that atmospheric Hg(0) exhibited a significant daily cycle with maximal
298 concentrations around noon. We show that this daily cycle occurred throughout the summer,
299 with low atmospheric Hg(0) concentrations ($\sim 0.50 \text{ ng/m}^3$) when solar radiation was
300 minimum and a maximum ($\sim 0.80 \text{ ng/m}^3$) around noon (see Fig. 7a). Such a pronounced daily
301 cycle has never been observed at other Antarctic stations (Dommergue et al., 2010;
302 Pfaffhuber et al., 2012). Several studies showed that Hg(0) emission from the snowpack
303 maximizes near midday (e.g., Steffen et al., 2002; Ferrari et al., 2005; Brooks et al., 2006;
304 Faïn et al., 2007; Ferrari et al., 2008; Johnson et al., 2008). As suggested by Durnford and
305 Dastoor (2011), the noon emission does not necessarily reflect maximum concentrations of
306 cryospheric Hg(0) around midday (Hg(0) concentration peaked in the afternoon at 10 cm
307 below the snow surface, see section 3.2.1) and could be driven by ventilation generated by
308 atmospheric thermal convection. Stable boundary layers are almost ubiquitous in Polar
309 Regions due to radiation cooling (Anderson and Neff, 2008). However, convective boundary

310 layers have been observed in summer at polar domes at Concordia Station (King et al., 2006)
311 and Summit in Greenland (Cohen et al., 2007). Fig. 7 displays the hourly mean variation of
312 several parameters. As illustrated by Figs. 7c and 7d, and in agreement with earlier
313 observations (Argentini et al., 2005; Pietroni et al., 2012; Argentini et al., 2013), there was a
314 strong diurnal cycle in near-surface temperature and wind speed in summer at Concordia
315 Station. These observations are typical for locations where a convective boundary layer
316 develops as a response to daytime heating (King et al., 2006), as can be seen in Fig. 7e. In a
317 convective boundary layer, vertical mixing is enhanced during convective hours (Anderson
318 and Neff, 2008), as shown in Figs. 7f and 7g by increasing values for the friction velocity (u_* ,
319 indicative of the strength of the mixing processes in the surface layer (Neff et al., 2008)) and
320 the Eddy diffusivity (K). Similarly, several studies highlighted that the atmospheric
321 turbulence at Concordia Station in summer influences the vertical flux and concentration
322 profiles of various atmospheric species (Legrand et al., 2009; Dommergue et al., 2012;
323 Kerbrat et al., 2012; Frey et al., 2013).

324 In summary, the observed summertime Hg(0) diurnal cycle in ambient air might be due to a
325 combination of factors: i) the intense oxidation of Hg(0) in ambient air due to the high
326 oxidative capacity on the plateau – as evidenced by low mean Hg(0) concentrations (see
327 section 3.2.1.a), ii) subsequent Hg(II) deposition onto snowpack – as evidenced by elevated
328 total mercury levels in surface snow samples (see section 3.2.1.a), and iii) emission of Hg(0)
329 from the snowpack during convective hours. Fig. 8 summarizes the processes that govern
330 mercury exchange at the air/snow interface. Redox processes occurring within the snowpack
331 are discussed in details in section 3.2.

332 **3.1.3 Fall**

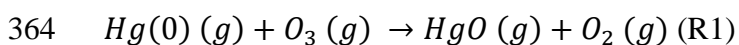
333 In fall, Hg(0) concentrations in ambient air no longer peaked around midday (see Fig. 7a) and
334 were in average 67% higher than during the summer, exceeding levels recorded at lower
335 latitudes in the Southern Hemisphere (Slemr et al., 2015). At this period of the year, the
336 boundary layer lowered to ~ 50 m in average and no longer exhibited a pronounced diurnal
337 cycle (see Figs. 3c and 7e). We believe that the shallow boundary layer could cause Hg(0)
338 concentrations in ambient air to build up to where they exceeded levels recorded at lower
339 latitudes in the Southern Hemisphere because Hg(0) – emitted from the snowpack – was
340 dispersed into a reduced volume of air, limiting the dilution. Similarly, NO_x mixing ratios are
341 enhanced when the boundary layer is shallow (Neff et al., 2008; Frey et al., 2013). Elevated

342 Hg(0) concentrations were also likely favored by the fact that oxidation in ambient air was
343 weaker under lower solar radiation.

344 **3.1.4 Winter**

345 While stable concentrations were expected in winter given the absence of photochemistry, our
346 observations reveal a 20 to 30% decrease of atmospheric Hg(0) concentrations from May to
347 mid-August (see Fig. 3a). Conversely, Hg(0) concentrations remained stable at Neumayer and
348 Troll from late fall through winter (Ebinghaus et al., 2002; Pfaffhuber et al., 2012). This
349 decreasing trend observed in winter might be due to several mechanisms, including gas-phase
350 oxidation, ~~and~~ heterogeneous reactions, or dry deposition of Hg(0).

351 Several studies suggested the involvement of nitrate radicals in the night-time oxidation of
352 Hg(0) (Mao and Talbot, 2012; Peleg et al., 2015). However, as previously mentioned, Dibble
353 et al. (2012) indicated that NO₃ binds Hg(0) too weakly to initiate its oxidation in the gas
354 phase. Another potential oxidant is O₃, with this reactant reaching a maximum in the winter
355 (see Fig. 3d). However, according to some theoretical studies (e.g., Hynes et al., 2009),
356 reaction (R1) is unlikely to proceed as a homogeneous reaction. Several experimental studies
357 confirmed the major product of reaction (R1) to be solid mercuric oxide, HgO (s) and not
358 HgO (g) (e.g., Pal and Ariya, 2004; Ariya et al., 2009), suggesting that pure gas phase
359 oxidation of elemental mercury by O₃ may not occur in the atmosphere. However, Calvert and
360 Lindberg (2005) proposed an alternative mechanism that would make this reaction potentially
361 viable in the atmosphere (Subir et al., 2011). The reaction may start with the formation of a
362 metastable HgO₃ (g) molecule which then decomposes to OHgOO (g) and thereafter
363 transforms to HgO (s) and O₂ (g).



365 As suggested by Subir et al. (2011), the influence of heterogeneous surfaces of water droplets,
366 snow, ice and aerosols should be taken into account when attempting to describe mercury
367 chemistry in the atmosphere. O'Concubhair et al. (2012) showed that freezing an acidic
368 solution containing nitrite or hydrogen peroxide can oxidize dissolved gaseous mercury in the
369 dark. Nitrous acid and hydrogen peroxide are present on the Antarctic plateau (Huey et al.,
370 2004; Hutterli et al., 2004). As suggested by Dommergue et al. (2012), similar processes
371 could occur in the snow or on surface hoar at Concordia Station in winter. In 2013, the height
372 of measurement had a significant influence on the decline over time of Hg(0) concentrations
373 (ANCOVA test, *p* value < 0.05), with a steeper decrease at 25 cm than at 1070 cm.

374 Additionally, wintertime Hg(0) concentrations were significantly lower at 25 cm than at 1070
375 cm (p value < 0.05, Mann-Whitney test). These results suggest that snowpack may act as a
376 sink for mercury, enhancing the deposition rate due to heterogeneous reactions, through
377 absorption of oxidation products, and/or physical sorption/condensation of Hg(0) on surface
378 snow.

379 The observed declining trend could also be attributed to the dry deposition of Hg(0) onto the
380 snowpack. The dry deposition velocity is defined as follows (Joffre, 1988), as the ratio
381 between the deposition flux F (ng/m²/s) and the concentration C (ng/m³):

$$382 \quad v_d = \frac{F}{C} \quad (2)$$

383 Denoting the height of the boundary layer h and the Hg(0) concentration at the beginning of
384 winter C_0 , the evolution of the concentration versus time is thus given by the following
385 ordinary differential equation:

$$386 \quad C = C_0 e^{-(v_d/h)t} \quad (3)$$

387 During winter ($t = 107$ days), the Hg(0) concentration gradually decreased from $C_0 \sim 1.03$
388 ng/m³ to $C \sim 0.73$ ng/m³ at 25 cm above the snowpack, in a mixing layer of 25 m high.
389 According to Equation (3) the associated dry deposition velocity is $9.3 \cdot 10^{-5}$ cm/s. This result
390 is in very good agreement with dry deposition velocities reported for Hg(0) over snow
391 (Cobbett et al., 2007; Zhang et al., 2009).

392 In spite of the observed decreasing trend of Hg(0) concentrations in ambient air, total mercury
393 concentrations in surface snow samples did not significantly increase over time in winter (see
394 Fig. 5). Using a snow density of 300 kg/m³ a loss of 0.30 ng/m³ over a period of three months
395 in a mixing layer of 25 m high would lead to a 2.5 ng/L increase in the first cm of the
396 snowpack. Given the variability of chemical species deposition onto the snow surface, and the
397 occurrence of either fresh snowfall or blowing snow, this 2.5 ng/L increase over a period of
398 three months could not be detected in our weekly surface snow samples.

399 Despite the overall decreasing trend in winter, Hg(0) concentration exhibited abrupt increases
400 when moist and warm air masses from lower latitudes occasionally reached Concordia
401 Station. This is, for example, evidenced on 13 June 2012 by an increase of 0.25 ng/m³ of the
402 Hg(0) concentration, an increase of temperature at 10 m a.g.l. from -63 to -26 °C, and a high
403 integrated water vapor column (see Fig. 9).

404 **3.2 Hg(0)/Hg(II) redox conversions within the snowpack**

405 The 2013 record of Hg(0) in the snow interstitial air (SIA) is displayed in Fig. 10. Fig. 11
406 depicts the mean Hg(0) concentration at various heights above and below the snow surface (in
407 the interstitial air of the snow) for all seasons.

408 **3.2.1 Sunlit period**

409 During the sunlit period (summer, spring/fall), Hg(0) concentration peaked in the upper layers
410 of the snowpack and then decreased with depth, with levels in the SIA dropping below
411 atmospheric values.

412 Hg(0) is generally produced in the upper layers of the snowpack – as the result of a
413 photolytically initiated reduction of Hg(II) (Lalonde et al., 2003) – and diffuses upward and
414 downward. According to our observations, Hg(0) concentration peaked at ~ 10 cm below the
415 snow surface (see Fig. 11). Similarly, Brooks et al. (2008) reported Hg(0) concentrations
416 peaking at a depth of 3 cm at South Pole. Below the top layer, the actinic flux decreases
417 exponentially with depth (King and Simpson, 2001; Domine et al., 2008). The light
418 penetration depth (*e*-folding depth) is the depth at which the actinic flux's magnitude is 1/*e* of
419 its incident value (Perovich, 2007). It is estimated that ~ 85% of the photoreduction occurs in
420 the top two *e*-folding depths (King and Simpson, 2001). At Concordia Station, the *e*-folding
421 depth is ~ 10 cm at 400 nm for the wind pack layers (France et al., 2011), which supports our
422 observations. Reduced mercury can concurrently be reoxidized within the snowpack. Below
423 the top layer, Hg(0) concentration in the SIA dropped with depth (see Fig. 11) suggesting that
424 oxidation dominated in the deepest layers – in good agreement with observations within the
425 snowpack at Kuujjuarapik/Whapmagoostui, Québec, Canada (Dommergue et al., 2003) –
426 leading to the formation of a Hg(II) reservoir.

427 The amount of Hg(0) emitted from the snowpack to the atmosphere (see section 3.1.2.c)
428 depends on the balance of reduction and oxidation processes within the upper layers of the
429 snowpack (Durnford and Dastoor, 2011). Fig. 12 depicts the hourly mean atmospheric and
430 interstitial air Hg(0) concentrations. Our observations indicate that summertime Hg(0)
431 concentration in the upper layers of the snowpack exhibited a diurnal cycle and peaked in the
432 afternoon (see Fig. 12a). Conversely, in spring/fall, Hg(0) concentration reached a maximum
433 at night and a minimum near midday in the upper layers of the snowpack (see Fig. 12b). The
434 balance of reduction and oxidation processes within the upper layers of the snowpack
435 suddenly shifted in summer. Similarly, Faïn et al. (2008) found that reduction dominated

436 during summer and oxidation in spring in the upper layers of the snowpack at Summit,
437 Greenland.

438 It is worth noting that Hg(0) concentration in the SIA was occasionally very high. For
439 instance, on 24 February 2013, Hg(0) concentration reached 3.00 ng/m^3 at a depth of 10 cm.
440 During this event, ice precipitation was observed at Concordia Station with depolarization
441 values greater than 30% (data not shown). This suggests that the presence of ice crystals could
442 enhance the dry deposition of Hg(II) species onto the snow surface leading to increased Hg(0)
443 formation in the upper layers of the snowpack. Indeed, due to an elevated specific surface
444 area, mercury-capture efficiency of ice crystals is high (Douglas et al., 2008). Unfortunately,
445 due to a low sampling frequency of surface snow samples (weekly), total mercury
446 concentrations cannot be used to study further the relationship between the occurrence of ice
447 precipitation events and dry deposition of mercury species.

448 **3.2.2 Winter**

449 Contrarily to the sunlit period, Hg(0) concentration increased with depth in the SIA in winter
450 (see Figs. 10 and 11). The average Hg(0) concentration amounted to 3.60 ng/m^3 at a depth of
451 70 cm and was observed at a temperature of about $-60 \text{ }^\circ\text{C}$ and not related to any change in
452 atmospheric composition. Our observations are in agreement with earlier studies indicating
453 that reduction of Hg(II) species is possible in the dark (Ferrari et al., 2004; Fain et al., 2007;
454 Ferrari et al., 2008). The production of Hg(0) might be due to the reduction of Hg(II) species
455 accumulated in the deepest layers of the snowpack during the sunlit period (see section 3.2.1).
456 This shift from oxidation to reduction in the deepest layers of the snowpack at the beginning
457 of winter remains unexplained.

458

459 **4 Implications at a continental scale**

460 Depletion events of atmospheric Hg(0) that have been observed in the Arctic and at various
461 coastal Antarctic stations have been associated with O_3 depletions, where Hg(0) and O_3
462 concentrations are positively correlated (Simpson et al., 2007). Increases in both Hg(II) and
463 Hg(p) have been reported in conjunction with decreases of Hg(0) (Lu et al., 2001; Lindberg
464 et al., 2002; Aspö et al., 2005). Conversely, low Hg(0) concentrations that were not
465 correlated or anti-correlated with O_3 were observed at Neumayer and Troll (Temme et al.,
466 2003; Pfaffhuber et al., 2012), while elevated Hg(II) concentrations (up to 0.33 ng/m^3) were
467 recorded at Terra Nova Bay in the absence of Hg(0)/ O_3 depletion (Sprovieri et al., 2002). The

468 intense oxidation of Hg(0) in summer (see section 3.1.2.a) and multi-day Hg(0) depletion
469 events observed at Concordia Station in January/February (see section 3.1.2.b) are expected to
470 result in the build-up of an inland atmospheric reservoir enriched in Hg(II) and depleted in
471 Hg(0) in the summer. Due to strong katabatic winds flowing out from the Antarctic Plateau –
472 generated by the negative buoyant force that develops in the stable cooled layer along the ice
473 sheet slopes (Gallée and Pettré, 1998) –, a fraction of this inland atmospheric reservoir can be
474 transported toward the coastal margin. The influence of the flows from the Antarctic plateau
475 on coastal locations varies depending on the location. As demonstrated by Parish and
476 Bromwich (1987) and Parish and Bromwich (2007), the volume of air moving off inland
477 Antarctica toward the coastal margin displays significant spatial variability due to the
478 topographic slope and orientation of the underlying ice sheets. Northward transport of air
479 from the plateau is enhanced in a few locations called confluence zones – e.g., the broad
480 region upslope from the Ross Ice Shelf at 175°E and the area near Adélie Land at 142°E – but
481 can be sporadically observed elsewhere explaining the aforementioned observations at
482 Neumayer, Troll, or Terra Nova Bay. Monitoring atmospheric mercury at a coastal station
483 situated close to a confluence zone could provide new insights regarding the extent of the
484 transport of reactive air masses from the Antarctic plateau. This topic is addressed in a
485 companion paper (Angot et al., 2016). The Antarctic continent shelters unconventional
486 atmospheric pathways of mercury reactivity both in winter and in summer. Its role should be
487 taken into account in the modeling of the global geochemical cycle of mercury.

488

489 **5 Conclusion**

490 Mean summertime atmospheric Hg(0) concentration was ~ 25% lower compared to values
491 recorded at other Antarctic stations at the same period of the year, suggesting an intense
492 oxidation of atmospheric Hg(0) within the shallow boundary layer as a result of the high
493 oxidative capacity of the Antarctic plateau atmosphere at this period of the year. This
494 hypothesis is further supported by high total mercury concentrations in surface snow samples
495 measured at the station (up to 74 ng/L). Our results confirm short-term observations by
496 Brooks et al. (2008) and Dommergue et al. (2012) of chemical exchange at the air/snow
497 interface. During the sunlit period, Hg(0) concentration peaked in the upper layers of the
498 snowpack. Summertime Hg(0) concentration in ambient air exhibited a pronounced diurnal
499 cycle likely due to large emissions from the snowpack as a response to daytime snowpack
500 ventilation. Our observations also reveal a decrease of atmospheric mercury concentrations in

501 winter (24-h darkness) possibly due to the dry deposition of Hg(0). Interestingly, this
502 decreasing trend has never been observed elsewhere. Additionally, Hg(0) concentrations
503 increased with depth in the snow interstitial air in winter likely due to a dark reduction of
504 Hg(II) species accumulated within the snowpack during the sunlit period. Finally, we reveal
505 the occurrence of multi-day to weeklong depletion events of Hg(0) in ambient air in summer,
506 that are not associated with depletion of O₃, and likely result from a stagnation of air masses
507 on the plateau triggering an accumulation of oxidants in the shallow boundary layer. This
508 behaviour is radically different from what is usually observed in the Arctic where only
509 mercury depletion events that were associated with O₃ depletion (and with a Hg(0)/O₃
510 correlation) have been highlighted so far. According to observations at coastal Antarctic
511 stations (see section 4), the reactivity observed at Concordia Station can be transported at a
512 continental scale by strong katabatic winds. Our understanding of the atmospheric mercury
513 chemistry on the Antarctic plateau is currently limited by the lack of continuous halogens
514 measurements. Our findings point out new directions for future kinetic, observational, and
515 modeling studies.

516

517 **Acknowledgements**

518 Mercury data reported in this paper are available upon request at
519 http://sdi.iaa.cnr.it/geoint/publicpage/GMOS/gmos_historical.zul. We thank A. Barbero and
520 the rest of the overwintering crew: S. Aubin, C. Lenormant, and R. Jacob. We also gratefully
521 acknowledge M. Barret for the development of a QA/QC software program, L. Bonato for the
522 analysis of total mercury in surface snow samples, D. Liptzin for the calculation of the
523 Obukhov length and friction velocity, M. Legrand for the 2012 ozone data, C. Genthon for the
524 meteorological data, E. Vignon for helpful discussion, and B. Jourdain and X. Faïn for their
525 help in the field. This work contributed to the EU-FP7 project Global Mercury Observation
526 System (GMOS – www.gmos.eu) and has been supported by a grant from Labex
527 OSUG@2020 (Investissements d’avenir – ANR10 LABX56), and the Institut Universitaire de
528 France. BQ and PR acknowledge ANR CLIMSLIP and HAMSTRAD Program 910,
529 respectively. Logistical and financial support was provided by the French Polar Institute IPEV
530 (Program 1028, GMOstral and Program 1011, SUNITEDC), and a grant from the U.S.
531 National Science Foundation (NSF, PLR#1142145). Computing resources for FLEXPART
532 simulations were provided by the IPSL CICLAD/CLIMSERV mesocenter. Meteorological
533 data were obtained thanks to LEFE/IMAGO programs CLAPA and GABLS4, IPEV program

534 CALVA/1013, and Observatoire des Sciences de l'Univers de Grenoble (GLACIOCLIM
535 observatory).

References

- Anderson, P. S., and Neff, W. D.: Boundary layer physics over snow and ice, *Atmospheric Chemistry and Physics*, 8, 3563-3582, 2008.
- Angot, H., Barret, M., Magand, O., Ramonet, M., and Dommergue, A.: A 2-year record of atmospheric mercury species at a background Southern Hemisphere station on Amsterdam Island, *Atmospheric Chemistry and Physics* 14, 11461-11473, 2014.
- Angot, H., Dion, I., Vogel, N., Magand, O., Legrand, M., and Dommergue, A.: Atmospheric mercury record at Dumont d'Urville, East Antarctic coast: continental outflow and oceanic influences, *Atmospheric Chemistry and Physics Discussions*, 10.5194/acp-2016-257, in review, 2016.
- Argentini, S., Viola, A., Sempreviva, A. M., and Petenko, I.: Summer boundary-layer height at the plateau site of Dome C, Antarctica, *Boundary-Layer Meteorology*, 115, 409-422, 2005.
- Argentini, S., Petenko, I., Viola, A., Mastrantonio, G., Pietroni, I., Casasanta, G., Aristidi, E., and Ghenton, C.: The surface layer observed by a high-resolution sodar at Dome C, Antarctica, *Annals of geophysics*, 56, doi:10.4401/ag-6347, 2013.
- Ariya, P. A., Peterson, K., Snider, G., and Amyot, M.: Mercury chemical transformation in the gas, aqueous and heterogeneous phases: state-of-the-art science and uncertainties, in: *Mercury fate and transport in the global atmosphere*, edited by: Pirrone, N., and Mason, R. P., Springer, New York, 2009.
- Aspmo, K., Gauchard, P.-A., Steffen, A., Temme, C., Berg, T., Bahlmann, E., Banic, C., Dommergue, A., Ebinghaus, R., Ferrari, C., Pirrone, N., Sprovieri, F., and Wibetoe, G.: Measurements of atmospheric mercury species during an international study of mercury depletion events at Ny-Ålesund, Svalbard, spring 2003. How reproducible are our present methods?, *Atmospheric Environment*, 39, 7607-7619, 2005.
- Bloom, N. S., and Fitzgerald, W. F.: Determination of volatile mercury species at the picogram level by low temperature gas chromatography with cold-vapor atomic fluorescence detection, *Analytica Chimica Acta*, 208, 151-161, 1988.
- Bocquet, F., Helmig, D., and Oltmans, S. J.: Ozone in interstitial air of the mid-latitude seasonal snowpack at Niwot Ridge, Colorado, Arctic, Antarctic, and Alpine Research, 39, 375-387, 2007.
- Brooks, S., Saiz-Lopez, A., Skov, H., Lindberg, S. E., Plane, J. M. C., and Goodsite, M. E.: The mass balance of mercury in the springtime arctic environment, *Geophysical research letters*, doi: 10.1029/2005GL025525, 2006.
- Brooks, S. B., Arimoto, R., Lindberg, S. E., and Southworth, G.: Antarctic polar plateau snow surface conversion of deposited oxidized mercury to gaseous elemental mercury with fractional long-term burial, *Atmospheric Environment*, 42, 2877-2884, 2008.
- Calvert, J. G., and Lindberg, S. E.: Mechanisms of mercury removal by O₃ and OH in the atmosphere, *Atmospheric Environment*, 39, 3355-3367, 2005.
- Cobbett, F. D., Steffen, A., Lawson, G., and Van Heyst, B. J.: GEM fluxes and atmospheric mercury concentrations (GEM, RGM and Hg(p)) in the Canadian Arctic at Alert, Nunavut, Canada (February–June 2005), *Atmospheric Environment*, 41, 6527-6543, <http://dx.doi.org/10.1016/j.atmosenv.2007.04.033>, 2007.

- Cohen, L., Helmig, D., Neff, W. D., Grachev, A. A., and Fairall, C. W.: Boundary-layer dynamics and its influence on atmospheric chemistry at Summit, Greenland, *Atmospheric Environment*, 5044-5060, 2007.
- D'Amore, F., Bencardino, M., Cinnirella, S., Sprovieri, F., and Pirrone, N.: Data quality through a web-based QA/QC system: implementation for atmospheric mercury data from the Global Mercury Observation System, *Environmental Science: Processes & Impacts*, 17, 1482-1491, 2015.
- Davis, D., Nowak, J. B., Chen, G., Buhr, M., Arimoto, R., Hogan, A., Eisele, F., Mauldin, L., Tanner, D., Shetter, R., Lefer, B., and McMurry, P.: Unexpected high levels of NO observed at South Pole, *Geophysical research letters*, 28, 3625-3628, 2001.
- Dibble, T. S., Zelic, M. J., and Mao, H.: Thermodynamics of reactions of ClHg and BrHg radicals with atmospherically abundant free radicals, *Atmospheric Chemistry and Physics*, 12, 10271-10279, 2012.
- Domine, F., Albert, M., Huthwelker, T., Jacobi, H.-W., Kokhanovsky, A. A., Lehning, M., Picard, G., and Simpson, W. R.: Snow physics as relevant to snow photochemistry, *Atmospheric Chemistry and Physics*, 8, 171-208, 2008.
- Dommergue, A., Ferrari, C. P., Gauchard, P.-A., and Boutron, C. F.: The fate of mercury species in a sub-arctic snowpack during snowmelt, *Geophysical research letters*, 30, 1621, 2003.
- Dommergue, A., Sprovieri, F., Pirrone, N., Ebinghaus, R., Brooks, S., Courteaud, J., and Ferrari, C. P.: Overview of mercury measurements in the antarctic troposphere, *Atmospheric Chemistry and Physics*, 10, 3309-3319, 2010.
- Dommergue, A., Barret, M., Courteaud, J., Cristofanelli, P., Ferrari, C. P., and Gallée, H.: Dynamic recycling of gaseous elemental mercury in the boundary layer of the antarctic plateau, *Atmospheric Chemistry and Physics*, 12, 11027-11036, 2012.
- Douglas, T. A., Sturm, M., Simpson, W. R., Blum, J. D., Alvarez-Aviles, L., Keeler, G. J., Perovich, D. K., Biswas, A., and Johnson, K.: Influence of snow and ice crystal formation and accumulation on mercury deposition to the Arctic, *Environmental Science and Technology*, 42, 1542-1551, 2008.
- Driscoll, C. T., Mason, R. P., Chan, H. M., Jacob, D. J., and Pirrone, N.: Mercury as a global pollutant: sources, pathways, and effects, *Environmental Science and Technology*, 47, 4967-4983, 2013.
- Durnford, D., and Dastoor, A.: The behavior of mercury in the cryosphere: a review of what we know from observations, *Journal of geophysical research*, 116, doi:10.1029/2010JD014809, 2011.
- Ebinghaus, R., Kock, H. H., Temme, C., Einax, J. W., Löwe, A. G., Richter, A., Burrows, J. P., and Schroeder, W. H.: Antarctic springtime depletion of atmospheric mercury, *Environmental Science and Technology*, 36, 1238-1244, 2002.
- Eisele, F., Davis, D. D., Helmig, D., Oltmans, S. J., Neff, W., Huey, G., Tanner, D., Chen, G., Crawford, J. H., Arimoto, R., Buhr, M., Mauldin, L., Hutterli, M., Dibb, J., Blake, D., Brooks, S. B., Johnson, B., Roberts, J. M., Wang, Y., Tan, D., and Flocke, F.: Antarctic tropospheric chemistry (ANTCI) 2003 overview, *Atmospheric Environment*, 2008, 2749-2761, 2008.
- Fäin, X., Grangeon, S., Bahlmann, E., Fritsche, J., Obrist, D., Dommergue, A., Ferrari, C., Cairns, W., Ebinghaus, R., Barbante, C., Cescon, P., and Boutron, C. F.: Diurnal production

of gaseous mercury in the alpine snowpack before snowmelt, *Journal of geophysical research*, 112, doi:10.1029/2007JD008520, 2007.

Faïn, X., Ferrari, C., Dommergue, A., Albert, M., Battle, M., Arnaud, L., Barnola, J.-M., Cairns, W., Barbante, C., and Boutron, C. F.: Mercury in the snow and firn at Summit Station, Central Greenland, and implications for the study of past atmospheric mercury levels, *Atmospheric Chemistry and Physics*, 8, 3441-3457, 2008.

Ferrari, C. P., Dommergue, A., Boutron, C. F., Skov, H., Goodsite, M. E., and Jensen, B.: Nighttime production of elemental gaseous mercury in interstitial air of snow at Station Nord, Greenland, *Atmospheric Environment*, 38, 2727-2735, 2004.

Ferrari, C. P., Gauchard, P.-A., Aspö, K., Dommergue, A., Magand, O., Bahlmann, E., Nagorski, S., Temme, C., Ebinghaus, R., Steffen, A., Banic, C., Berg, T., Planchon, F., Barbante, C., Cescon, P., and Boutron, C. F.: Snow-to-air exchanges of mercury in an arctic seasonal snowpack in Ny-Alesund, Svalbard, *Atmospheric Environment*, 39, 7633-7645, 2005.

Ferrari, C. P., Padova, C., Faïn, X., Gauchard, P.-A., Dommergue, A., Aspö, K., Berg, T., Cairns, W., Barbante, C., Cescon, P., Kaleschke, L., Richter, A., Wittrock, F., and Boutron, C. F.: Atmospheric mercury depletion event study in Ny-Alesund (Svalbard) in spring 2005. Deposition and transformation of Hg in surface snow during springtime, *Science of the Total Environment*, 397, 167-177, 2008.

Fitzgerald, W. F., and Gill, G. A.: Subnanogram determination of mercury by two-stage gold amalgamation and gas detection applied to atmospheric analysis, *Analytical chemistry*, 51, 1714-1720, 1979.

France, J. L., King, M. D., Frey, M. M., Erbland, J., Picard, G., Preunkert, S., MacArthur, A., and Savarino, J.: Snow optical properties at Dome C (Concordia), Antarctica; implications for snow emissions and snow chemistry of reactive nitrogen, *Atmospheric Chemistry and Physics*, 11, 9787-9801, 2011.

Frey, M. M., Brough, N., France, J. L., Anderson, P. S., Traulle, O., King, M. D., Jones, A. E., Wolff, E. W., and Savarino, J.: The diurnal variability of atmospheric nitrogen oxides (NO and NO₂) above the Antarctic Plateau driven by atmospheric stability and snow emissions, *Atmospheric Chemistry and Physics*, 13, 3045-3062, 2013.

Frey, M. M., Roscoe, H. K., Kukui, A., Savarino, J., France, J. L., King, M. D., Legrand, M., and Preunkert, S.: Atmospheric nitrogen oxides (NO and NO₂) at Dome C, East Antarctica, during the OPALE campaign, *Atmospheric Chemistry and Physics*, 15, 7859-7875, 2015.

Gallée, H., and Pettré, P.: Dynamical constraints on katabatic wind cessation in Adélie Land, Antarctica, *Journal of the atmospheric sciences*, 55, 1755-1770, 1998.

Gallée, H., and Gorodetskaya, I. V.: Validation of a limited area model over Dome C, Antarctic Plateau, during winter, *Climate Dynamics*, 34, 61-72, 2010.

Gallée, H., Preunkert, S., Argentini, S., Frey, M. M., Genthon, C., Jourdain, B., Pietroni, I., Casasanta, G., Barral, H., Vignon, E., Amory, C., and Legrand, M.: Characterization of the boundary layer at Dome C (East Antarctica) during the OPALE summer campaign, *Atmospheric Chemistry and Physics*, 15, 6225-6236, 2015.

Genthon, C., Town, M. S., Six, D., Favier, V., Argentini, S., and Pellegrini, A.: Meteorological atmospheric boundary layer measurements and ECMWF analyses during summer at Dome C, Antarctica, *Journal of geophysical research*, 115, D05104, 2010.

- Genthon, C., Six, D., Gallée, H., Grigioni, P., and Pellegrini, A.: Two years of atmospheric boundary layer observations on a 45-m tower at Dome C on the Antarctic plateau, *Journal of geophysical research: atmospheres*, 118, 3218-3232, 2013.
- Goodsite, M. E., Plane, J. M. C., and Skov, H.: A theoretical study of the oxidation of Hg^0 to HgBr_2 in the troposphere, *Environmental Science and Technology*, 38, 1772-1776, 2004.
- Grannas, A. M., Jones, A. E., Dibb, J., Ammann, M., Anastasio, C., Beine, H. J., Bergin, M., Bottenheim, J., Boxe, C. S., Carver, G., Chen, G., Crawford, J. H., Domine, F., Frey, M. M., Guzman, M. I., Heard, D. E., Helmig, D., Hoffmann, M. R., Honrath, R. E., Huey, L. G., Hutterli, M., Jacobi, H.-W., Klan, P., Lefer, B., McConnell, J. R., Plane, J. M. C., Sander, R., Savarino, J., Shepson, P. B., Simpson, W. R., Sodeau, J., Von Glasow, R., Weller, R., Wolff, E. W., and Zhu, T.: An overview of snow photochemistry: evidence, mechanisms and impacts, *Atmospheric Chemistry and Physics*, 7, 4329-4373, 2007.
- Hedgecock, I. M., and Pirrone, N.: Chasing quicksilver: modeling the atmospheric lifetime of $\text{Hg}(0)$ in the marine boundary layer at various latitudes, *Environmental Science and Technology*, 38, 69-76, 2004.
- Hoegstroem, U.: Non-dimensional wind and temperature profiles in the atmosphere surface layer: a re-evaluation, *Boundary-Layer Meteorology*, 42, 55-78, 1988.
- Holmes, C. D., Jacob, D. J., and Yang, X.: Global lifetime of elemental mercury against oxidation by atomic bromine in the free troposphere, *Geophysical research letters*, 33, 2006.
- Huey, L. G., Tanner, D. J., Slusher, D. L., Dibb, J. E., Arimoto, R., Chen, G., Davis, D., Buhr, M. P., Nowak, J. B., Mauldin, L., Eisele, F. L., and Kosciuch, E.: CIMS measurements of HNO_3 and SO_2 at the South Pole during ISCAT 2000, *Atmospheric Environment*, 38, 5411-5421, 2004.
- Hutterli, M. A., McConnell, J. R., Chen, G., Bales, R. C., Davis, D. D., and Lenschow, D. H.: Formaldehyde and hydrogen peroxide in air, snow and interstitial air at South Pole, *Atmospheric Environment*, 38, 5439-5450, 2004.
- Hynes, A. J., Donohoue, D. L., Goodsite, M. E., and Hedgecock, I. M.: Our current understanding of major chemical and physical processes affecting mercury dynamics in the atmosphere and at the air-water/terrestrial interfaces, in: *Mercury fate and transport in the global atmosphere*, edited by: Pirrone, N., and Mason, R. P., Springer, New York, 427-457, 2009.
- Joffre, S. M.: Modelling the dry deposition velocity of highly soluble gases to the sea surface, *Atmospheric Environment* (1967), 22, 1137-1146, [http://dx.doi.org/10.1016/0004-6981\(88\)90343-5](http://dx.doi.org/10.1016/0004-6981(88)90343-5), 1988.
- Johnson, K. P., Blum, J. D., Keeler, G. J., and Douglas, T. A.: Investigation of the deposition and emission of mercury in arctic snow during an atmospheric mercury depletion event, *Journal of geophysical research*, 113, doi: 10.1029/2008JD009893, 2008.
- Kerbrat, M., Legrand, M. P., S., Gallée, H., and Kleffmann, J.: Nitrous acid at Concordia (inland site) and Dumont d'Urville (coastal site), east antarctica, *Journal of geophysical research*, 117, doi:10.1029/2011JD017149, 2012.
- King, J. C., and Anderson, P. S.: Heat and water vapor fluxes and scalar roughness lengths over an Antarctic ice shelf, *Boundary-Layer Meteorology*, 69, 101-121, 1994.
- King, J. C., Argentini, S. A., and Anderson, P. S.: Contrasts between the summertime surface energy balance and boundary layer structure at Dome C and Halley stations, Antarctica, *Journal of geophysical research*, 111, doi:10.1029/2005JD006130, 2006.

- King, M. D., and Simpson, W. R.: Extinction of UV radiation in Arctic snow at Alert, Canada (82°N), *Journal of geophysical research* 106, 12499-12507, 2001.
- Kukui, A., Legrand, M., Preunkert, S., Frey, M. M., Loisil, R., Gil Roca, J., Jourdain, B., King, M. D., France, J. L., and Ancellet, G.: Measurements of OH and RO₂ radicals at Dome C, East Antarctica, *Atmospheric Chemistry and Physics*, 14, 12373-12392, 2014.
- Lalonde, J. D., Amyot, M., Doyon, M.-R., and Auclair, J.-C.: Photo-induced Hg(II) reduction in snow from the remote and temperate experimental lakes area (Ontario, Canada), *Journal of geophysical research*, 108, doi:10.1029/2001JD001534, 2003.
- Lambert, G., Ardouin, B., and Sanak, J.: Atmospheric transport of trace elements toward Antarctica, *Tellus B*, 42, 76-82, 10.1034/j.1600-0889.1990.00009.x, 1990.
- Legrand, M., Preunkert, S., Jourdain, B., Gallée, H., Goutail, F., Weller, R., and Savarino, J.: Year-round record of surface ozone at coastal (Dumont d'Urville) and inland (Concordia) sites in east antarctica, *Journal of geophysical research*, 114, doi:10.1029/2008JD011667, 2009.
- Legrand, M. P., S., Savarino, J., Frey, M. M., Kukui, A., Helmig, D., Jourdain, B., Jones, A., Weller, R., Brough, N., and Gallée, H.: Inter-annual variability of surface ozone at coastal (Dumont d'Urville, 2004-2014) and inland (Concordia, 2007-2014) sites in East Antarctica, *Atmospheric Chemistry and Physics*, doi:10.5194/acp-2016-95, in press, 2016.
- Lin, C.-J., and Pehkonen, S. O.: The chemistry of atmospheric mercury: a review, *Atmospheric Environment*, 33, 2067-2079, 1999.
- Lin, C.-J., Pan, L., Streets, D. G., Shetty, S. K., Jang, C., Feng, X., Chu, H.-W., and Ho, T. C.: Estimating mercury emission outflow from East Asia using CMAQ-Hg, *Atmospheric Chemistry and Physics*, 10, 1856-1864, 2010.
- Lindberg, S. E., Brooks, S., Lin, C.-J., Scott, K. J., Landis, M. S., Stevens, R. K., Goodsite, M. E., and Richter, A.: Dynamic oxidation of gaseous mercury in the arctic troposphere at polar sunrise, *Environmental Science and Technology*, 36, 1245-1256, 2002.
- Lu, J. Y., Schroeder, W. H., Barrie, L. A., Steffen, A., Welch, H. E., Martin, K., Lockhart, L., Hunt, R. V., Boila, G., and Richter, A.: Magnification of atmospheric mercury deposition to polar regions in springtime: the link to tropospheric ozone depletion chemistry, *Geophysical research letters*, 28, 3219-3222, 2001.
- Mao, H., and Talbot, R.: Speciated mercury at marine, coastal, and inland sites in New England - Part 1: Temporal variability, *Atmospheric Chemistry and Physics*, 12, 5099-5112, 2012.
- Mason, R. P., Choi, A. L., Fitzgerald, W. F., Hammerschmidt, C. R., Lamborg, C. H., Soerensen, A. L., and Sunderland, E. M.: Mercury biogeochemical cycling in the ocean and policy implications, *Environmental Research*, 119, 101-117, 2012.
- Munthe, J., Sprovieri, F., Horvat, M., and Ebinghaus, R.: SOPs and QA/QC protocols regarding measurements of TGM, GEM, RGM, TPM and mercury in precipitation in cooperation with WP3, WP4 and WP5. GMOS deliverable 6.1, CNR-IIA, IVL. <http://www.gmos.eu>, last access: 3 March 2014, 2011.
- Neff, W., Helmig, D., Grachev, A. A., and Davis, D.: A study of boundary layer behavior associated with high NO concentrations at the South Pole using a minisodar, tethered balloon, and sonic anemometer, *Atmospheric Environment*, 42, 2762-2779, 2008.
- O'Concubhair, R., O'Sullivan, D. A., and Sodeau, J. R.: Dark oxidation of dissolved gaseous mercury in polar ice mimics, *Environmental Science and Technology*, 46, 2012.

- Pal, B., and Ariya, P. A.: Studies of ozone initiated reactions of gaseous mercury: kinetics, product studies, and atmospheric implications, *Physical Chemistry Chemical Physics*, 6, 572-579, 2004.
- Parish, T. R., and Bromwich, D. H.: The surface windfield over the Antarctic ice sheets, *Nature*, 328, 51-54, 1987.
- Parish, T. R., and Bromwich, D. H.: Reexamination of the near-surface airflow over the Antarctic continent and implications on atmospheric circulations at high southern latitudes, *Monthly Weather Review*, 135, 1961-1973, 2007.
- Peleg, M., Tas, E., Obrist, D., Matveev, V., Moore, C., Gabay, M., and Luria, M.: Observational evidence for involvement of nitrate radicals in nighttime oxidation of mercury, *Environmental Science and Technology*, 49, 14008-14018, 2015.
- Perovich, D. K.: Light reflection and transmission by a temperate snow cover, *Journal of glaciology*, 53, 201-210, 2007.
- Pfaffhuber, K. A., Berg, T., Hirdman, D., and Stohl, A.: Atmospheric mercury observations from Antarctica: seasonal variation and source and sink region calculations, *Atmospheric Chemistry and Physics*, 12, 3241-3251, 2012.
- Pietroni, I., Argentini, S., Petenko, I., and Sozzi, R.: Measurements and parametrizations of the atmospheric boundary-layer height at Dome C, Antarctica, *Boundary-Layer Meteorology*, 143, 189-206, 2012.
- Ricaud, P., Grigioni, P., Zbinden, R., Attié, J.-L., Genoni, L., Galeandro, A., Moggio, L., Montaguti, S., Petenko, I., and Legovini, P.: Review of tropospheric temperature, absolute humidity and integrated water vapor from the HAMSTRAD radiometer installed at Dome C, Antarctica, 2009-14, *Antarctic Science*, 27, 598-616, 2015.
- Schroeder, W. H., Anlauf, K. G., Barrie, L. A., Lu, J. Y., Steffen, A., Schneeberger, D. R., and Berg, T.: Arctic springtime depletion of mercury, *Nature*, 394, 331-332, 1998.
- Seok, B., Helmig, D., Williams, M. W., Liptzin, D., and Chowanski, K. H., J.: An automated system for continuous measurements of trace gas fluxes through snow: an evaluation of the gas diffusion method at a subalpine forest site, Niwot Ridge, Colorado, *Biogeochemistry*, 95, 95-113, 2009.
- Simpson, W. R., Von Glasow, R., Riedel, K., Anderson, P. S., Ariya, P. A., Bottenheim, J., Burrows, J. P., Carpenter, L. J., Friess, U., Goodsite, M. E., Heard, D. E., Hutterli, M., Jacobi, H.-W., Kaleschke, L., Neff, W., Plane, J. M. C., Platt, U., Richter, A., Roscoe, H. K., Sander, R., Shepson, P. B., Sodeau, J., Steffen, A., Wagner, T., and Wolff, E. W.: Halogens and their role in polar boundary-layer ozone depletion, *Atmospheric Chemistry and Physics*, 7, 4375-4418, 2007.
- Slemr, F., Angot, H., Dommergue, A., Magand, O., Barret, M., Weigelt, A., Ebinghaus, R., Brunke, E.-G., Pfaffhuber, K. A., Edwards, G., Howard, D., Powell, J., Keywood, M., and Wang, F.: Comparison of mercury concentrations measured at several sites in the Southern Hemisphere, *Atmospheric Chemistry and Physics*, 15, 3125-3133, 2015.
- Sprovieri, F., Pirrone, N., Hedgecock, I. M., Landis, M. S., and Stevens, R. K.: Intensive atmospheric mercury measurements at Terra Nova Bay in Antarctica during November and December 2000, *Journal of geophysical research*, 107, 4722, 2002.
- Steffen, A., Schroeder, W., Bottenheim, J., Narayan, J., and Fuentes, J. D.: Atmospheric mercury concentrations: measurements and profiles near snow and ice surfaces in the Canadian Arctic during Alert 2000, *Atmospheric Environment*, 36, 2653-2661, 2002.

Steffen, A., Douglas, T., Amyot, M., Ariya, P. A., Aspmo, K., Berg, T., Bottenheim, J., Brooks, S., Cobbett, F., Dastoor, A., Dommergue, A., Ebinghaus, R., Ferrari, C., Gardfeldt, K., Goodsite, M. E., Lean, D., Poulain, A. J., Scherz, C., Skov, H., Sommar, J., and Temme, C.: A synthesis of atmospheric mercury depletion event chemistry in the atmosphere and snow, *Atmospheric Chemistry and Physics*, 8, 1445-1482, 2008.

Steffen, A., Scherz, T., Oslon, M., Gay, D. A., and Blanchard, P.: A comparison of data quality control protocols for atmospheric mercury speciation measurements, *Journal of Environmental Monitoring*, 14, 752-765, doi: 10.1039/c2em10735j, 2012.

Stohl, A., Hittenberger, M., and Wotawa, G.: Validation of the Lagrangian particle dispersion model FLEXPART against large scale tracer experiments, *Atmospheric Environment*, 32, 4245-4264, 1998.

Stohl, A., and Thomson, D. J.: A density correction for Lagrangian particle dispersion models, *Boundary-Layer Meteorology*, 90, 155-167, 1999.

Stohl, A., Forster, C., Frank, A., Seibert, P., and Wotawa, G.: Technical note: the Lagrangian particle dispersion model FLEXPART version 6.2, *Atmospheric Chemistry and Physics*, 5, 2461-2474, 2005.

Subir, M., Ariya, P. A., and Dastoor, A.: A review of uncertainties in atmospheric modeling of mercury chemistry I. Uncertainties in existing kinetic parameters - fundamental limitations and the importance of heterogeneous chemistry, *Atmospheric Environment*, 45, 5664-5675, 2011.

Tekran: Tekran 2537 mercury monitor detection limit. Summary of known estimates, Tekran Instruments Corp., Toronto, ON, Canada., 2011.

Temme, C., Einax, J. W., Ebinghaus, R., and Schroeder, W. H.: Measurements of atmospheric mercury species at a coastal site in the antarctic and over the atlantic ocean during polar summer, *Environmental Science and Technology*, 37, 22-31, 2003.

UNEP: Text of the Minamata Convention on Mercury for adoption by the Conference of Plenipotentiaries. [unep.org. July 31, Available at: http://www.unep.org/hazardoussubstances/Portals/9/Mercury/Documents/dipcon/CONF_3_Minamata%20Convention%20on%20Mercury_final%2026%2008_e.pdf](http://www.unep.org/hazardoussubstances/Portals/9/Mercury/Documents/dipcon/CONF_3_Minamata%20Convention%20on%20Mercury_final%2026%2008_e.pdf), last access: 27 March 2016, 2013.

Wang, F., Saiz-Lopez, A., Mahajan, A. S., Gomez Martin, J. C., Armstrong, D., Lemes, M., Hay, T., and Prados-Roman, C.: Enhanced production of oxidised mercury over the tropical pacific ocean: a key missing oxidation pathway, *Atmospheric Chemistry and Physics*, 14, 1323-1335, 2014.

Weiss-Penzias, P., Jaffe, D. A., Swartzendruber, P., Hafner, W., Chand, D., and Prestbo, E.: Quantifying Asian and biomass burning sources of mercury using the Hg/CO ratio in pollution plumes observed at the Mount Bachelor observatory, *Atmospheric Environment*, 41, 4366-4379, 2007.

Xiao, W., Liu, S., Li, H., Xiao, Q., Wang, W., Hu, Z., Hu, C., Gao, Y., Shen, J., Zhao, X., Zhang, M., and Lee, X.: A flux-gradient system for simultaneous measurement of the CH₄, CO₂, and H₂O fluxes at a lake-air interface, *Environmental Science and Technology*, 48, 14490-14498, 2014.

Zhang, L., Wright, L. P., and Blanchard, P.: A review of current knowledge concerning dry deposition of atmospheric mercury, *Atmospheric Environment*, 43, 5853-5864, 2009.

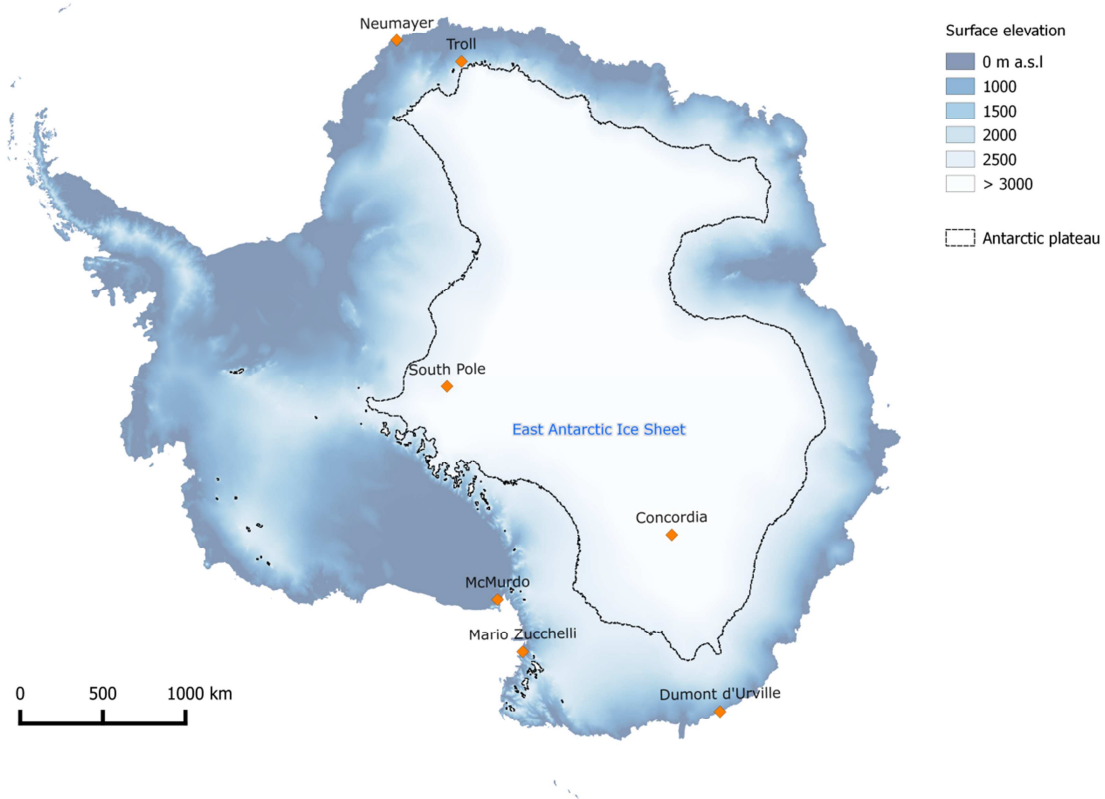
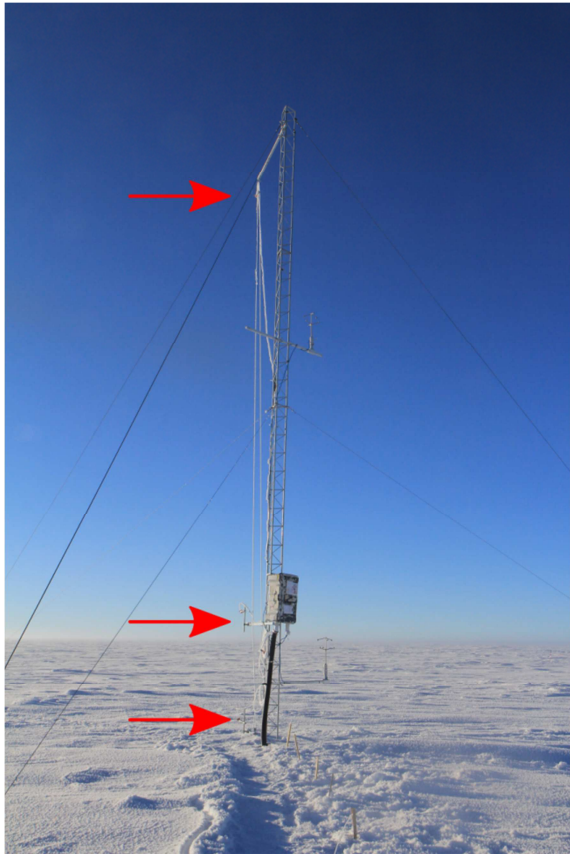


Figure 1: Map of Antarctica showing surface elevation (meters above sea level, m a.s.l) and the position of stations where atmospheric mercury measurements have been performed with modern on-line instruments. The black line shows the periphery of the high altitude plateau (> 2500 m a.s.l).

a)



b)



Figure 2: Photographs showing **a)** the meteorological tower with the three gas inlets (red arrows) at 1070 cm, 210 cm and 25 cm above the snow surface (photo credit: B. Jourdain), and **b)** one of the snow towers with the two sampling inlets above the snowpack at 50 and 10 cm (photo credit: D. Helmig).

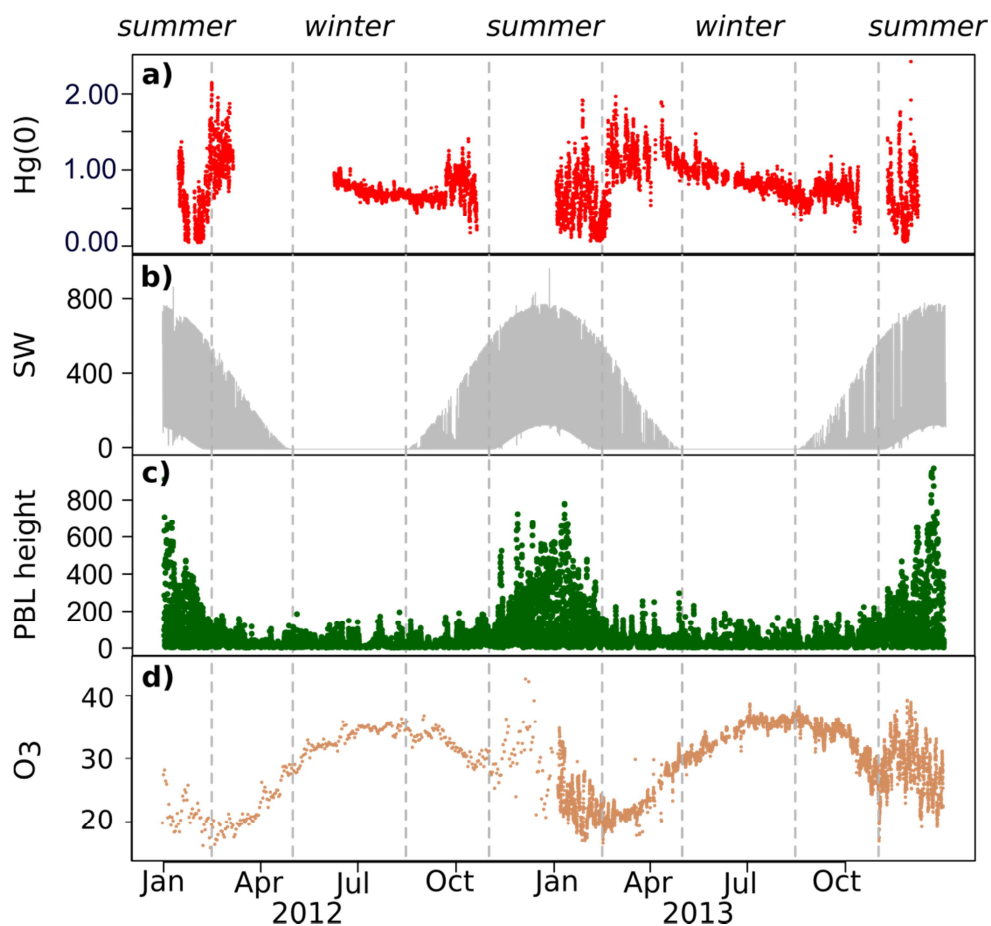


Figure 3: Annual variation in 2012 and 2013 of **a)** hourly-averaged Hg(0) concentrations (in ng/m^3) at 500 cm and 25 cm above the snow surface in 2012 and 2013, respectively, **b)** downwelling shortwave (SW) radiation (in W/m^2), **c)** planetary boundary layer (PBL) height (in m), and **d)** ozone (O_3 , daily mean in 2012 and hourly mean in 2013) mixing ratios (in ppbv). The vertical dashed lines represent seasonal boundaries.

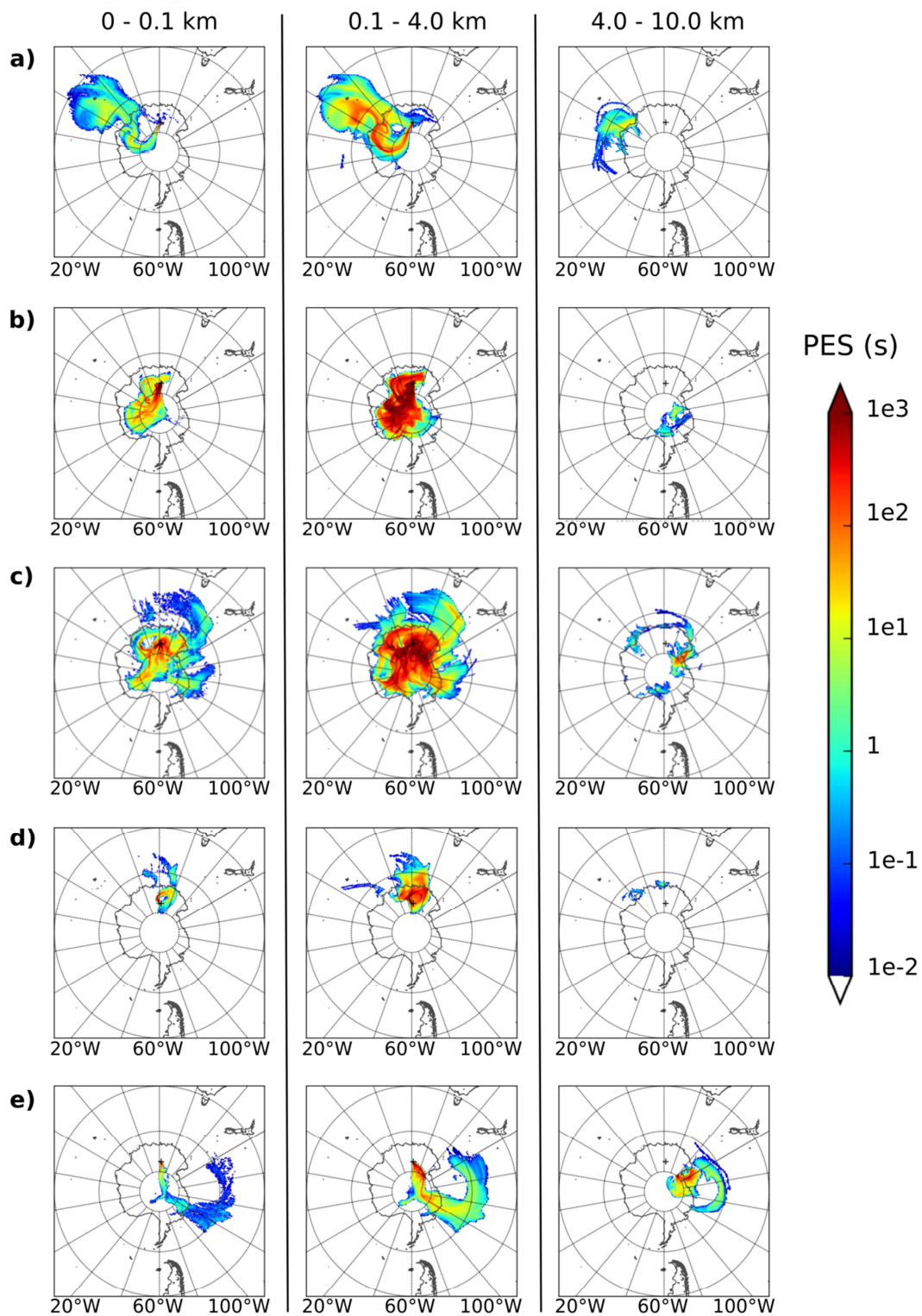


Figure 4: Back trajectories for the 3 layers of altitude colored according to the potential emission sensitivity (PES, in seconds) **a)** on 11 September 2013, **b)** from 19 January to 8 February 2012, **c)** from 5 to 20 February 2013, **d)** on 10 February 2012, and **e)** on 22 February 2013. Note that PES in a particular grid cell is proportional to the particle residence time in that cell.

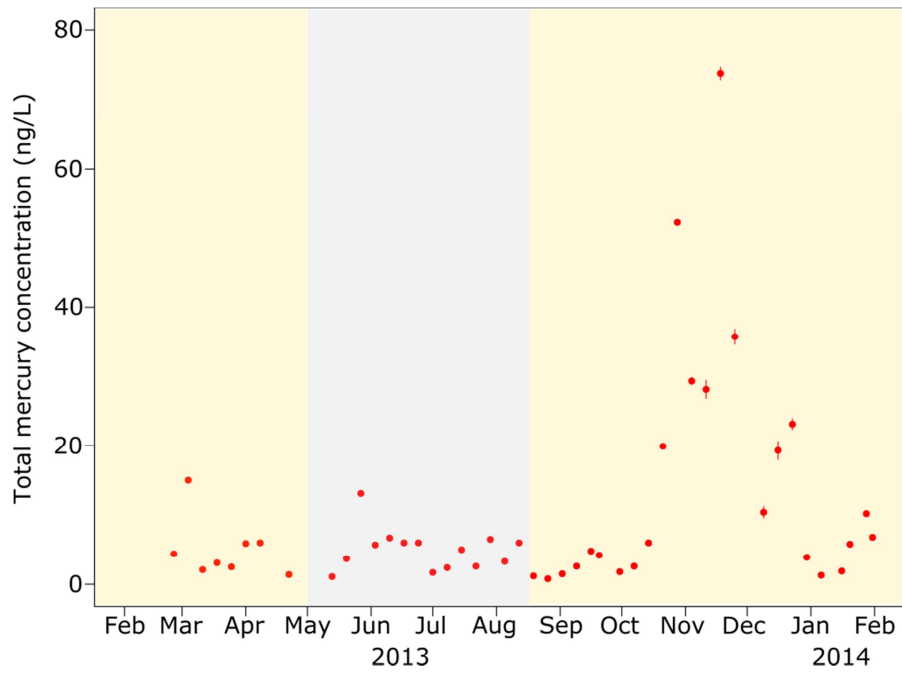


Figure 5: Total mercury concentration (ng/L), along with standard errors, in surface snow samples collected weekly at Concordia Station from February 2013 to January 2014. Dark period (winter) highlighted in grey, sunlit period highlighted in yellow. Total mercury concentrations were elevated (up to 74 ng/L) in November-December 2013 (summer). All samples were analyzed in replicates of three. Standard errors are frequently smaller than the width of the dots.

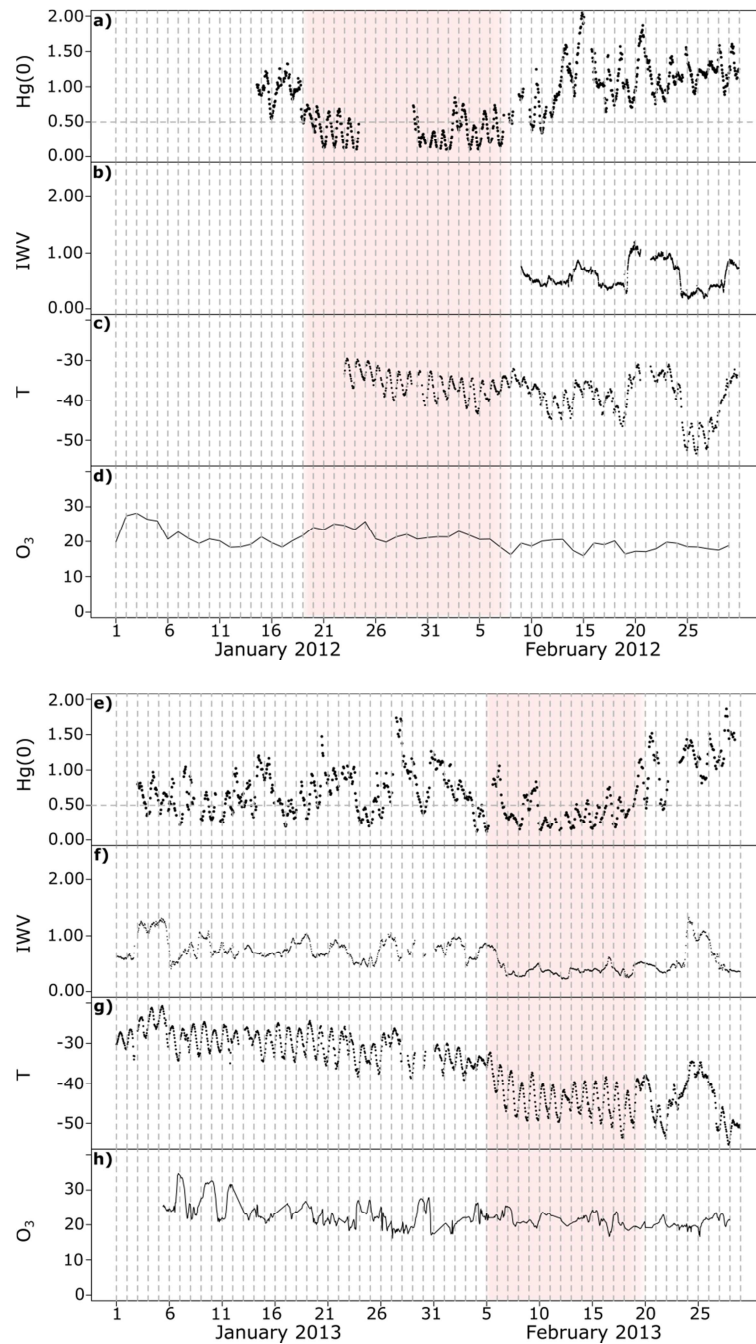


Figure 6: Top: January and February 2012 cycle of: **a)** hourly-averaged Hg(0) concentrations (in ng/m^3) at 500 cm above the snow surface, **b)** Integrated Water Vapor (IWV, kg/m^2), **c)** Temperature (in $^\circ\text{C}$) at 10 m above ground level, and **d)** ozone (O_3 , daily mean) mixing ratios (ppbv). Hg(0) was low from 19 January to 8 February (period highlighted in red) while O_3 showed no abnormal variability. Bottom: January and February 2013 cycle of: **e)** hourly-averaged Hg(0) concentrations (in ng/m^3) at 210 cm above the snow surface, **f)** Integrated Water Vapor (IWV, kg/m^2), **g)** Temperature (in $^\circ\text{C}$) at 10 m above ground level, and **h)** ozone (O_3 , hourly mean) mixing ratio (ppbv). Hg(0), IWV, and temperature were low from 5 to 20 February (period highlighted in red) while O_3 showed no abnormal variability. Note that Hg(0) concentrations exhibited the same pattern at the three inlets of the meteorological tower from 5 to 20 February 2013.

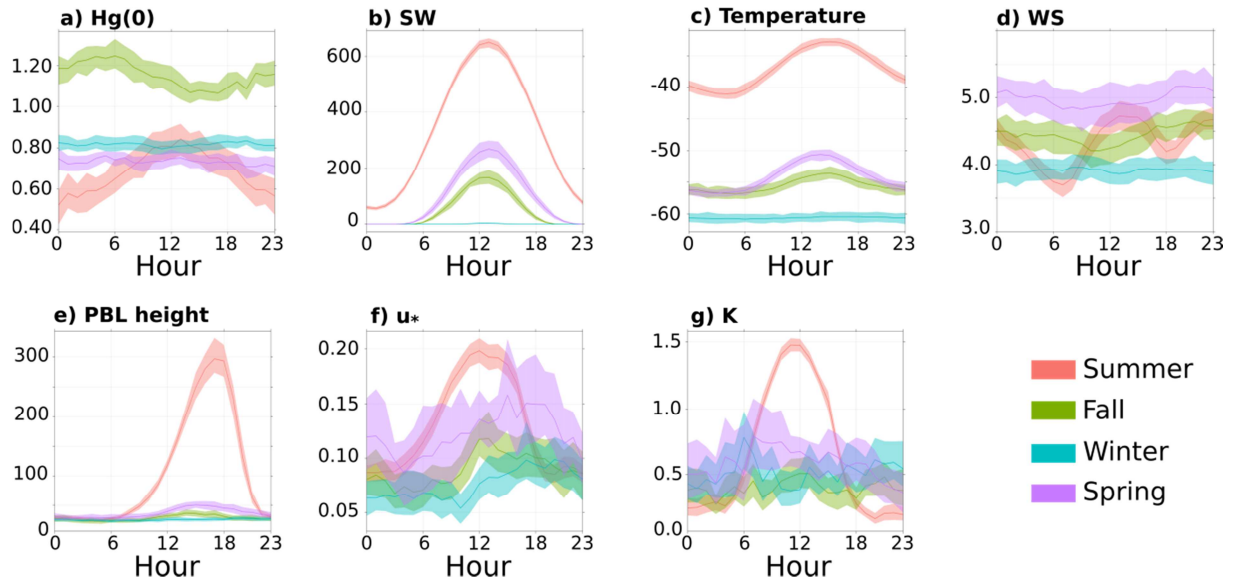


Figure 7: Hourly (local time) mean variation, along with the 95% confidence interval for the mean, of: **a)** Hg(0) concentration (in ng/m^3) at 25 cm above the snow surface, **b)** downwelling shortwave (SW) radiation (in W/m^2) according to the MAR model simulations, **c)** temperature (in $^\circ\text{C}$) at 3 m above the snow surface, **d)** wind speed at 3 m above the snow surface (in m/s), **e)** planetary boundary layer (PBL) height (in m) according to the MAR model simulations, **f)** friction velocity (u_* , in m/s), and **g)** Eddy diffusivity (K , in m^2/s) in summer (red), fall (green), winter (blue), and spring (purple). Note that the hourly mean variation of Hg(0) concentration in summer is similar at the three inlets of the meteorological tower.

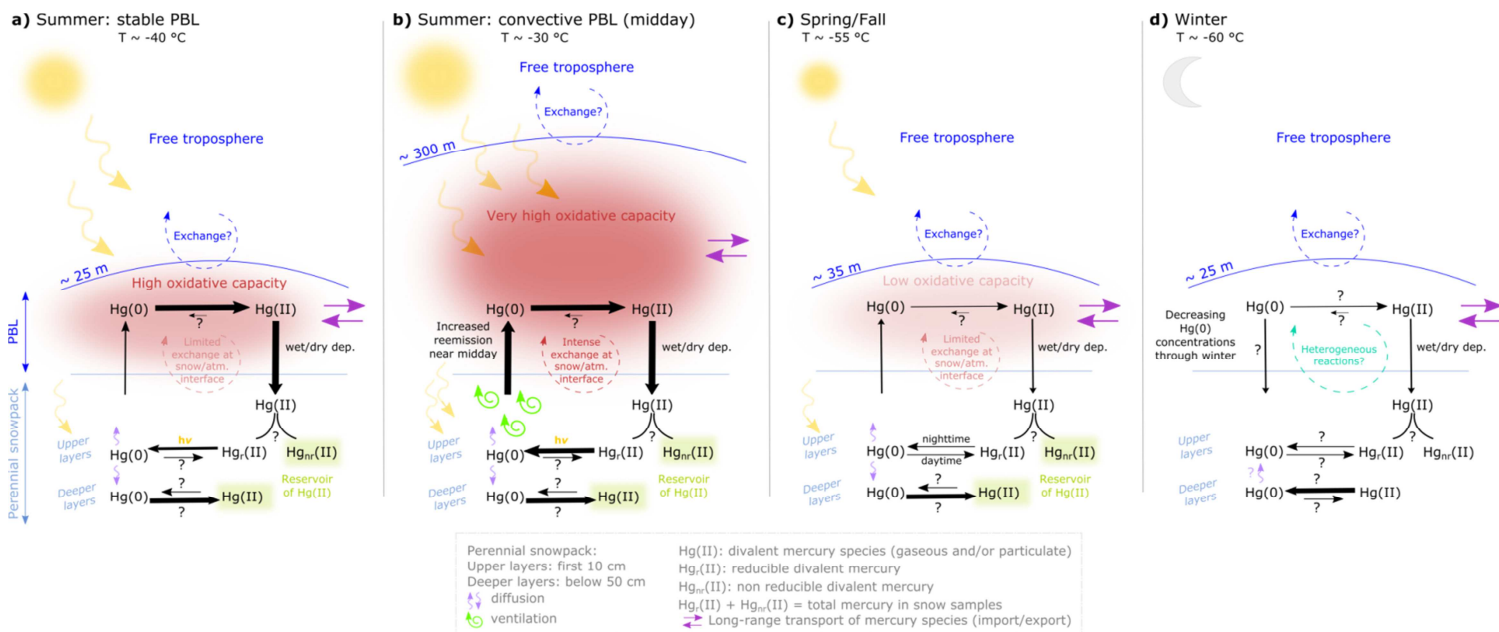


Figure 8: Schematic diagram illustrating the processes that govern the Hg(0) budget at Concordia Station **a)** in summer under stable Planetary Boundary Layer (PBL) conditions, **b)** in summer under convective PBL conditions, **c)** in spring/fall, and **d)** in winter. In summer, Hg(0) is continuously intensely oxidized due to the high oxidative capacity of the boundary layer and a large amount of divalent mercury species deposit onto the snowpack. A fraction of deposited mercury can be reduced (the reducible pool, Hg_r(II)) in the upper layers of the snowpack and subsequently reemitted to the atmosphere as Hg(0). Hg(0) emission from the snowpack maximizes near midday likely due to increased ventilation as a response to daytime heating. Oxidation of Hg(0) dominates in the deeper layers of the snowpack likely leading to the formation of a Hg(II) reservoir. In spring/fall, the balance of reduction and oxidation processes within the upper layers of the snowpack differs from summertime: oxidation dominates during the day, reduction at night. In winter, Hg(0) is produced in the deeper layers of the snowpack likely as a result of the reduction of Hg(II) species accumulated during the sunlit period. Ambient Hg(0) concentrations exhibit a 20 to 30% decrease through winter possibly due to dry deposition of Hg(0).

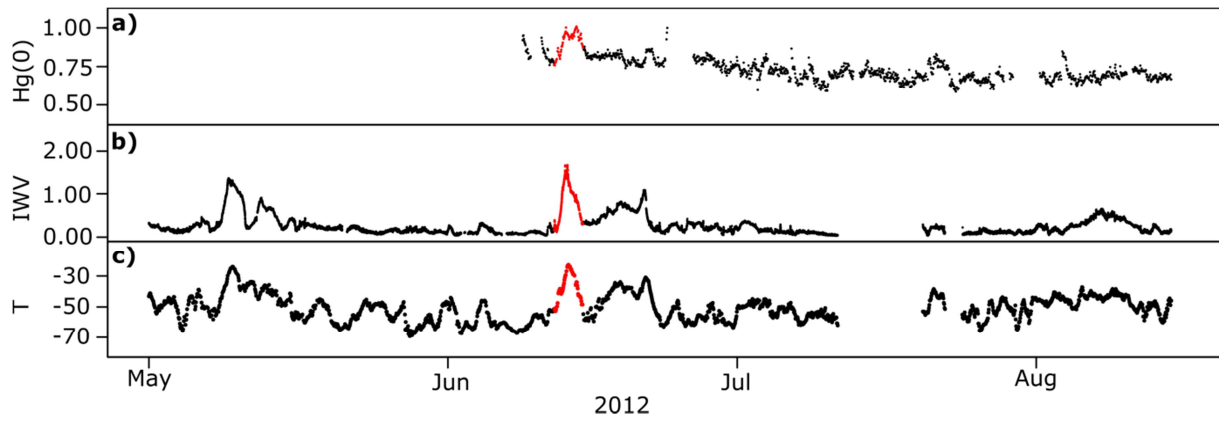


Figure 9: Year 2012 wintertime record of: **a)** hourly-averaged Hg(0) concentrations (in ng/m^3) at 500 cm above the snow surface, **b)** Integrated Water Vapor (IWV, kg/m^2), and **c)** Temperature (T, $^{\circ}\text{C}$) at 10 m above ground level. Hg(0), temperature, and IWV increased from June 12 to 15 (in red) suggesting transport of moist and warm air masses originating from lower latitudes.

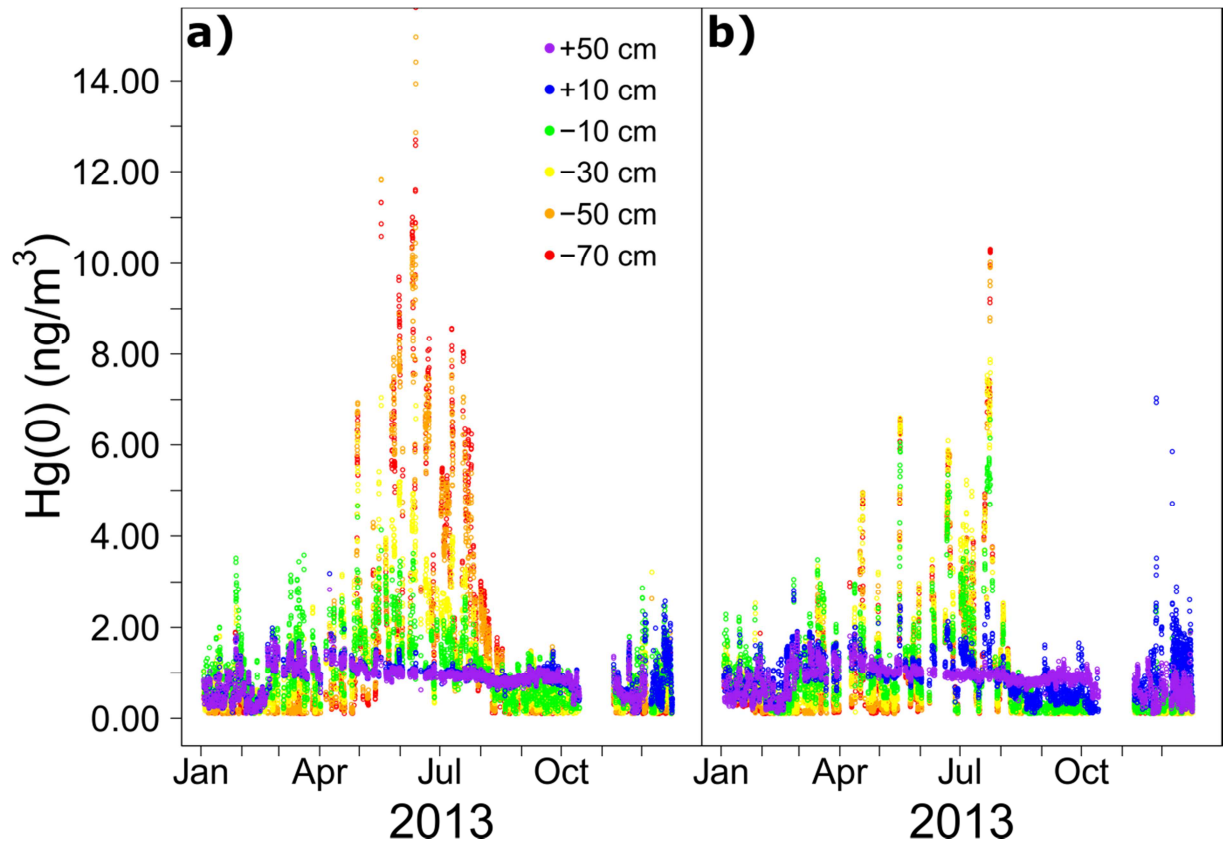


Figure 10: Annual variation of hourly-averaged Hg(0) concentrations (in ng/m^3) in the snow interstitial air collected at the various inlets of the two snow towers: **a)** snow tower #1, **b)** snow tower #2. Note that we regularly experienced technical problems on snow tower #2 leading to missing values.

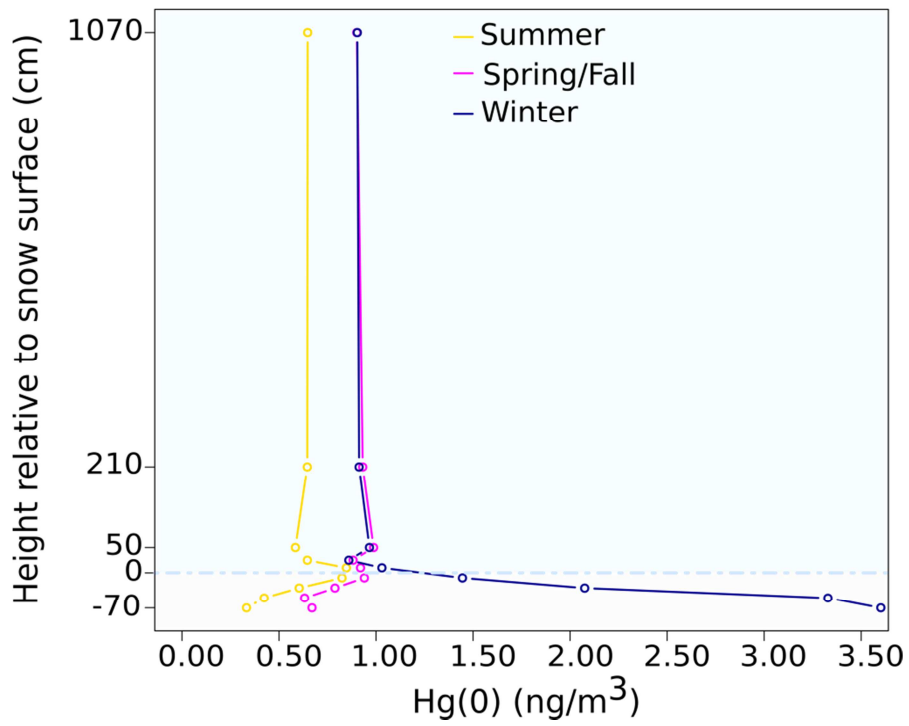


Figure 11: Mean Hg(0) concentration (ng/m^3) measured at various heights above and below the snow surface (cm) at Concordia Station in summer (yellow), spring/fall (purple), and winter (dark blue) The horizontal light blue dashed line represents the snow surface.

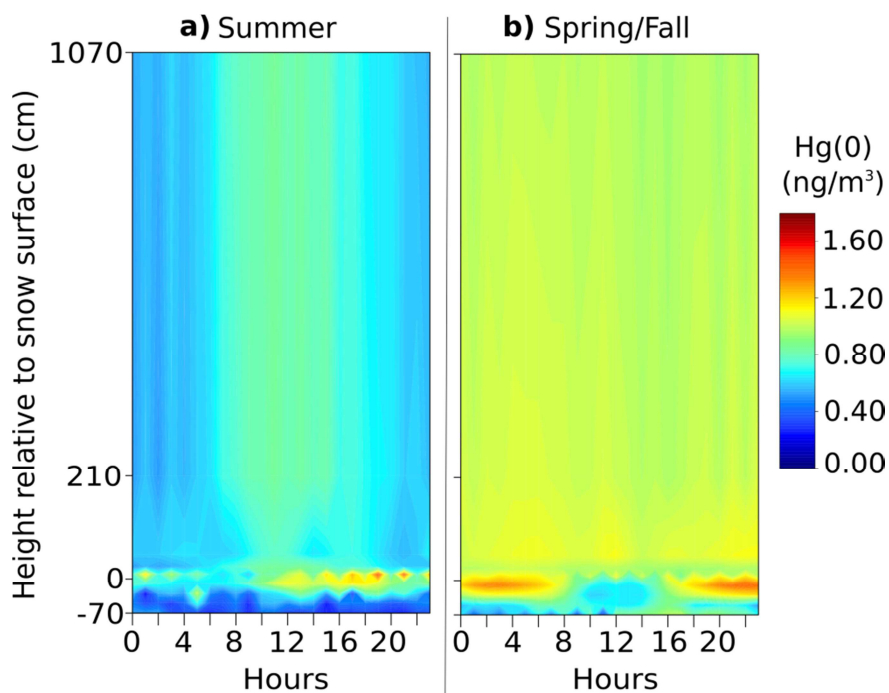


Figure 12: Hourly (local time) mean atmospheric and interstitial air Hg(0) concentrations in **a)** summer, and **b)** spring/fall. The vertical axis is the height of measurement relative to the snow surface (in cm). Color contours show Hg(0) concentrations (in ng/m^3). Concentrations at 25, 210, and 1070 cm above the snow surface were acquired on the meteorological tower while concentrations at 50, 10, -10, -30, -50 cm, and -70 cm were collected on snow tower #1. Data were cubic spline interpolated using software R.